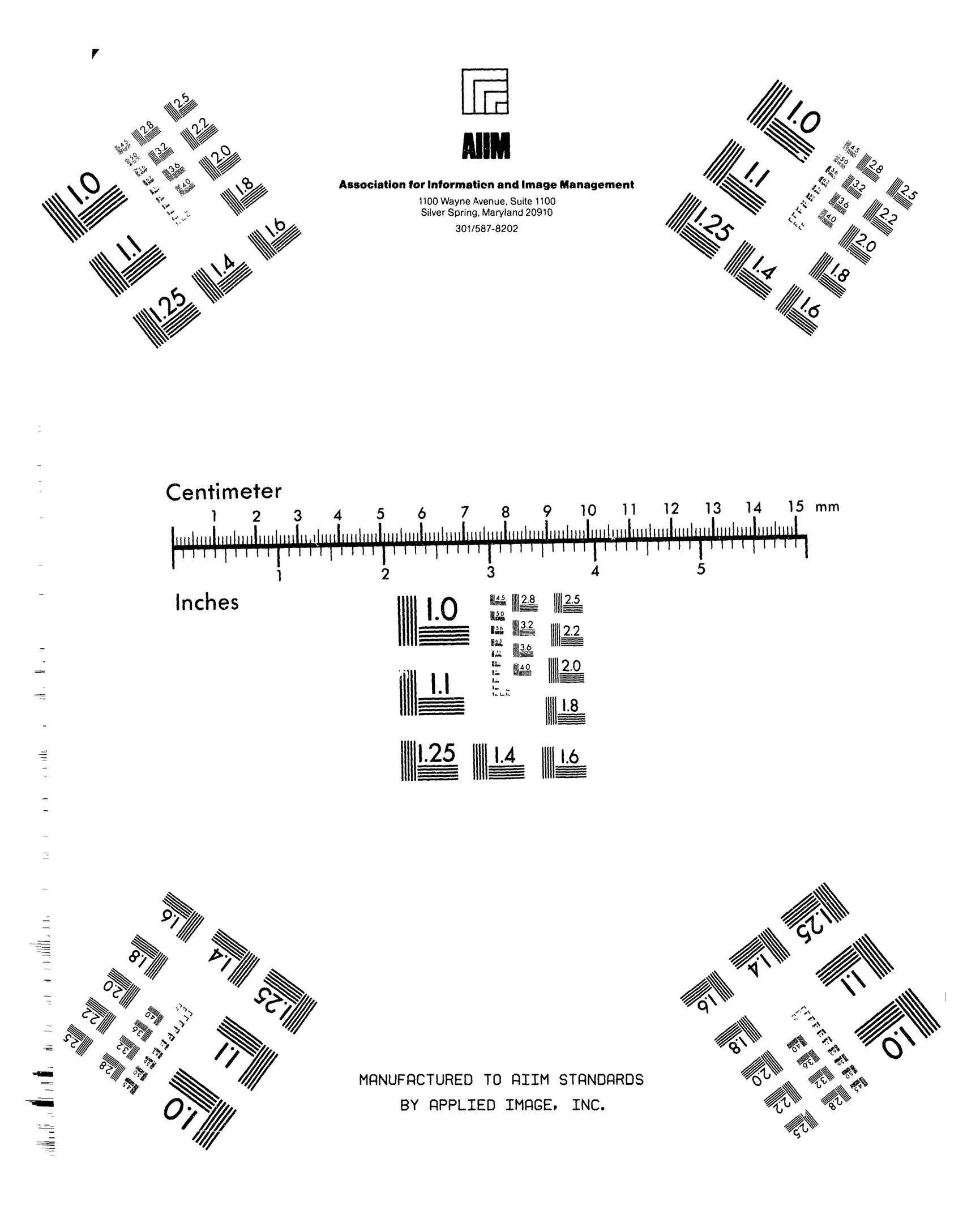
AIIM
Association for Information and Image Management
1100 Wayne Avenue, Suite 1100
Silver Spring, Maryland 20910
301/587-8202
Centimeter
Inches
MANUFACTURED TO AIIM STANDARDS
BY APPLIED IMAGE, INC.

1 of 1

Abstract

Our research funded by the Department of Energy has involved the characterization of catalyst acidity, ^{2}D NMR studies of Brønsted acid sites, and kinetic, calorimetric, and spectroscopic studies of methylamine synthesis and related reactions over acid catalysts. The approach of this work has been to explore quantitative correlations between the factors that control the generation, type, strength, and catalytic properties of acid sites on zeolite catalysts. Our systematic studies involving microcalorimetry, thermogravimetric analysis, IR spectroscopy, and NMR spectroscopy have provided important information about the nature and strength of acid sites in zeolites. Furthermore, this information has been vital in understanding the catalytic cycles involved in methylamine synthesis and related reactions over zeolite catalysts. We propose to continue our NMR investigations of Brønsted acid sites in zeolites and related catalysts. In addition, we will continue to employ methylamine synthesis and related reactions to probe solid acid catalysts. Furthermore, microcalorimetry will remain an important technique to study the chemical bonding of basic molecules with acid sites. In the longer term, we will extend these techniques to investigate other solid acid catalyst systems, such as AlPO's, SAPO's, and solid superacids. We will also begin to investigate the alkylation of toluene with methanol and the alkylation of isobutane with light olefins. These reactions are of interest because of the need for new generations of solid acid alkylation catalysts to replace liquid acids for environmental reasons.

Introduction

During the past three years our research has involved (1) characterization of catalyst acidity using microcalorimetry, infrared spectroscopy, thermogravimetric analysis, and temperature-programmed desorption, (2) development of deuterium NMR techniques to probe the nature of Brønsted acid sites in zeolites, (3) kinetic studies of methylamine synthesis and related reactions over acid catalysts, (4) calorimetric and spectroscopic studies of the adsorption of reactants and products of methylamine synthesis on zeolites, and (5) formulation and analysis of catalytic cycles for methylamine synthesis and related reactions on acid catalysts. The results of our efforts in each of these directions are summarized in Sections II-VI. The proposed directions of our future work are outlined in Section VII.

Characterization of Catalyst Acidity

Introduction

The characterization of catalyst acidity has been a continuing research direction that our group has followed in our work funded by the Department of Energy. Our work began with calorimetric studies of pyridine adsorption on a series of silica-supported metal oxides and

DISCLAIMER

progressed to include the adsorption of ammonia, trimethylamine, and triethylamine on selected silica-supported metal oxides. During the past three years, we have investigated a series of zeolite catalysts, including HNa-Y zeolites, H-mordenite, several H-ZSM-5 zeolites, and a series of steamed fluid cracking catalysts.

Quantitative characterization of catalyst acidic properties is important for elucidation of the role of acidity in determining catalytic properties. Characterization of the acid sites involves determining the strength of the sites, the mobility of molecules adsorbed on the sites, the number of sites, and the type of acid site. A measure of acid strength is provided by the heat of adsorption of a probe molecule on the acid site. A thermodynamic representation of surface mobility is given by the standard entropy change of adsorption. Acid site type refers to Brønsted or Lewis classifications.

We have used microcalorimetry, thermogravimetric analysis, and temperature-programmed desorption to study the acidity of various zeolites. Microcalorimetry is used to measure heats of adsorption of probe molecules on the acid site, providing information about both the acid strength and the strength distribution. Thermogravimetric analysis measures the number of adsorbed probe molecules on acid sites over a wide range of temperatures and pressures. Standard entropy changes of adsorption are obtained by combining the results of this technique with microcalorimetric measurements of adsorption heats. The main purpose of temperature-programmed desorption in our work has been to compare quantitatively the results from these techniques.

Selected Calorimetric Results

Figures 1-3 show representative calorimetric data in the form of the differential heat of pyridine adsorption versus the amount of pyridine adsorbed on the catalyst. Figure 1 shows that the H-ZSM-5 sample studied (provided by W. Haag at Mobil, with Si/Al~35) has an apparently uniform acid-strength distribution, giving an average heat of ~180 kJ/mol. The acid-strength distribution of H-mordenite is also apparently rather uniform, as shown in Figure 2, with an average heat of pyridine adsorption equal to ~200 kJ/mol. This sample appears to have a small number of very strong acid sites that we believe may be Lewis acid centers associated with non-framework aluminum species. Figure 3 shows that the acid strength distribution of HNa-Y zeolite is more heterogeneous than that of H-ZSM-5 or H-mordenite. This result is probably due to the lower Si/Al ratio of this HNa-Y sample (~2.4), leading to weaker acid sites corresponding to protons associated with framework Al species having one or more next-nearest-neighbor Al cations.

The microcalorimetric results of ammonia adsorption on H-mordenite and H-ZSM-5 are shown in Figure 4. As observed for pyridine, the curves of the differential heat of ammonia adsorption versus coverage are dominated by plateaus of constant differential heat, indicative of a large number of sites of similar acid strength. Ammonia, however, shows a lower value for the heat of adsorption than pyridine, in accordance with the lower gas-phase basicity of ammonia. On H-mordenite and H-ZSM-5 most of the acid sites have a heat of adsorption equal to 157 and 150 kJ/mol,

respectively. At higher coverages, ammonia is adsorbed weakly, at a strength of adsorption approximately equivalent to ammonia adsorption on silica.

Temperature-Programmed Desorption

Figure 5 shows a temperature-programmed desorption spectrum of ammonia from H-ZSM-5. This spectrum is dominated by a desorption feature centered at 611 K. This figure also shows a computer simulation of the TPD experiment, obtained by solving the differential equations that describe desorption and readsorption of ammonia on the acid sites. In these simulations, the desorption activation energy was set equal to the differential heat of adsorption determined by microcalorimetry. A standard preexponential factor of 10^{13} s^{-1} was assumed for the desorption step. The standard entropy change of adsorption, the only adjustable parameter used to fit the experimental spectrum, was determined to have a value of -172 J/mol-K. The breadth of the spectrum is not fully described by the simulation, and this result may be due to some readsorption of ammonia on walls of the apparatus. The simulated ammonia desorption spectrum for H-mordenite gives a value of the standard entropy change of adsorption equal to -164 J/mol-K.

Ammonia TPD spectra were collected for H-mordenite by varying the sample size for two sets of carrier-gas flowrate (0.42 and 1.25 cm^3/s) to extract the enthalpy and entropy of adsorption. The results of these experiments are presented in Figure 6 as a plot of $2\ln T_m - \ln(W/F)$ versus $1/T_m$. Here W is the catalyst weight (g), F is the carrier-gas flowrate (cm^3/s) measured at room temperature, and T_m is the temperature corresponding to the desorption-peak maximum. The slope of this plot is equal to $-\Delta H_{ads}/R$, assuming that adsorption and desorption are equilibrated during the TPD experiment, as indicated by our more general TPD simulations. Good agreement was obtained between the two series of runs with an average heat of ammonia adsorption on H-mordenite equal to 153 ± 3 kJ/mol. This value agrees well with the microcalorimetric result for ammonia adsorption on the same H-mordenite sample. The intercept of the above plot is equal to $\ln[-A_0 T_0 \beta \Delta H_{ads}(1-\theta_m)^2/P_0] + \Delta S^\circ_{ads}/R$, where A_0 is the acid site density (mol/g), T_0 is room temperature, P_0 is the standard state pressure (1 bar), and θ_m is the surface coverage at temperature T_m. The value of the standard entropy change extracted from the intercept of Figure 6 is equal to -156 J/mol-K. This value compares favorably with the value of -164 J/mol-K determined above from analysis of a single desorption experiment and utilizing the heat of adsorption determined calorimetrically.

The gas-phase absolute entropy of ammonia at 473 K and a pressure of 1 bar is 208 J/mol-K, of which 153 J/mol-K correspond to translational entropy. Thus, the entropy change of adsorption, ΔS°_{ads} = -172 J/mol-K, for H-ZSM-5 corresponds to a loss of translational entropy, with preservation of most of the rotational and vibrational entropy. Similarly, for H-mordenite the entropy change of adsorption, ΔS°_{ads} = -164 J/mol-K, corresponds to a loss

of translational entropy with essentially no loss of rotational and vibrational entropy.

Equilibration of Bases on Acid Sites

An important consideration in the interpretation of calorimetric data for adsorption of strong bases such as pyridine on zeolites is whether the molecules equilibrate with the acid sites, providing a good measure of the acid-strength distribution. At the temperature that our calorimetric adsorption studies were conducted, 473 K, the adsorption of pyridine is irreversible, and equilibration of pyridine on the acid sites by adsorption/desorption processes is not rapid. Thus, surface diffusion appears to be the primary mode by which equilibration of pyridine could take place. However, as suggested to us by Professor Hall (University of Pittsburgh), the extent to which pyridine may equilibrate with the acid sites remains an open question. Accordingly, we have recently conducted several experiments to provide additional information about whether the acid-strength distribution for H-ZSM-5 is homogeneous, in contrast to being heterogeneous as suggested by thermogravimetric measurements conducted by Deeba and Hall [1, 2] for pyridine adsorption on a series of amorphous silica/alumina catalysts.

Our first experiments involved thermogravimetric studies of pyridine adsorption on an H-ZSM-5 sample with a Si/Al ratio of 33. Chemical analysis of the sample showed 452 ± 20 μmol/g Al, 8 ± 1 μmol/g K, and 36 ± 2 μmol/g Na. Magic-angle spinning ^{27}Al NMR identified 14.9±2.0 % of the aluminum cations as present in octahedral coordination, the balance being tetrahedrally coordinated.

Thermogravimetric measurements were obtained using a quartz-spring (Ruska Instruments) microbalance. Prior to pyridine adsorption, the sample was first calcined at 723 K for 5 h in flowing oxygen, followed by an overnight evacuation at this temperature. Doses of pyridine were then introduced into the microbalance system. The flow of pyridine into the system was adjusted to a rate sufficient to maintain approximately the desired pressure of pyridine over the sample.

Thermogravimetric data were collected in the form of two isobars at 20 and 50 mTorr of pyridine, spanning a temperature range from 473 to 733 K, and one isotherm at 523 K between pyridine pressures of 20 mTorr and 5 Torr. The thermogravimetric data collected in this manner are shown in Figure 7. The total number of sites, based on the maximum pyridine uptake, was 463 μmol/g.

Microcalorimetric measurements of pyridine adsorption indicated that this sample contains a large number of Brønsted acid sites of apparently homogeneous strength, a significant number of weaker adsorption sites caused by alkali exchange cations, and some hydrogen-bonding sites associated with some dealumination of the sample. The thermogravimetric data are in agreement with the calorimetric results, as evidenced by the plateau near 320 μmol/g for the two isobars, followed by the further increase in the amount adsorbed with increasing pressure at 523 K. Specifically, a broad distribution of adsorption strengths would give rise to a

monotonic increase in the amount of adsorbed pyridine with decreasing temperature and increasing pressure.

The results of dimethyl ether adsorption on H-ZSM-5 are shown in Figure 8. Unlike pyridine, which has a high gas-phase proton affinity of 922 kJ/mol, dimethyl ether is a weak base with a proton affinity of 808 kJ/mol. Accordingly, the adsorption of dimethyl ether at temperatures near 400 K is reversible, and this weak base should provide a good assessment of the acid-strength distribution. The observation that the heat of adsorption of this molecule is relatively constant with respect to the amount adsorbed is thus important evidence that the acid-strength distribution of this H-ZSM-5 sample is, in fact, rather homogeneous.

The data of Figure 3 suggest that microcalorimetric measurements can be used to probe acid-strength distribution, since a rather broad range of heats of adsorption is observed for an HNa-Y zeolite having a low Si/Al ratio, where a range of acid strengths is expected. We have investigated this HNa-Y zeolite sample further by conducting microcalorimetry measurements of ammonia adsorption. This basic molecule is smaller than pyridine and adsorbs more weakly.

An HNa-Y zeolite sample with 82 % of the Na exchange cations replaced by protons was heated slowly under vacuum to 573 K, heated slowly in oxygen to 723 K, and then held at this temperature for 4 h. The cell was subsequently evacuated to 10^{-5} Torr for 2 h at 723 K and then cooled under vacuum to either 423 or 473 K, at which temperatures calorimetric measurements of ammonia adsorption were made. The results of these measurements are shown in Figure 9, in which the differential heat of adsorption is plotted as a function of coverage for ammonia adsorption at 423 K. The initial heat of adsorption is near 140 kJ/mol, but it decreases to a plateau at 120 kJ/mol. This curve shows that there are a few strong sites (~500 μmol/g), which are saturated with the first few doses of ammonia. The plateau which follows is a result of a series of sites having similar strength. Once these sites are saturated (beyond 1500 μmol/g), the heat decreases again to a second plateau at about 80 kJ/mol.

Superimposed on this calorimetric plot are isosteric heats of adsorption collected independently by Boudart [3] and co-workers, using thermogravimetric analysis and the Clausius-Clapeyron relation. The heat of ammonia adsorption on HNa-Y zeolite measured by microcalorimetry agrees very well with the values determined thermogravimetrically, except at extremely low coverage. This excellent agreement provides evidence that microcalorimetry can be used to probe the acid-strength distribution of this sample.

In an attempt to reconcile the broad range of acid strengths observed by Deeba and Hall [1, 2] for a series of silica/alumina catalysts, we have conducted microcalorimetric experiments of ammonia adsorption on γ-alumina. A sample of γ-alumina (Davison) was treated in oxygen for 4 h at 723 K, followed by evacuation for 2 h at this temperature. The sample cell was then placed in the calorimeter, and calorimetric data for ammonia and pyridine adsorption were subsequently collected at 423 and 473 K, respectively. The results of these microcalorimetric measurements are

shown in Figure 10. Evidence is seen here for a monotonic decrease in the heat of adsorption versus coverage. Superimposed on this plot are isosteric heats of pyridine adsorption collected thermogravimetrically by Deeba and Hall [2]. The agreement is good between the results of these calorimetric and thermogravimeric measurments. These authors also suggested that the heats of pyridine and ammonia adsorption were similar on such a sample. The observed decrease in heat of adsorption versus coverage may indicate a distribution of adsorption sites for this sample (e.g., aluminum cations with various extents of coordinative unsaturation) or adsorbate-adsorbate interactions present at the relatively high surface coverages reached for this sample. It is clear from these results, however, that microcalorimetric measurements can show a distribution of adsorption heats for appropriate samples.

Concluding Remark

We have continued to conduct systematic and quantitative studies of catalyst acidity. During the past three years, these studies have focused primarily on zeolite catalysts. We have compared carefully the results obtained from several different techniques applied to a variety of samples. While the quantitative assessment of acidity and the acid-strength distribution remains a subject for further research, we believe that careful microcalorimetric and thermogravimetric analyses can be used to compare the acidic properties of a wide variety of acidic materials. As such, our future work will deal less with studying these quantitative methods for acidity characterization, and we will focus more on using these techniques to probe the acidity of novel catalytic materials, e.g., materials for alkylation processes, where liquid acids must be replaced for environmental reasons.

Deuterium NMR Studies of Brønsted Acidity

Introduction

Nuclear magnetic resonance spectroscopy has proved useful in studies of many aspects of zeolites. ^{29}Si and ^{27}Al NMR are now routinely used to characterize the zeolitic framework. ^{13}C and ^{1}H spectroscopies of adsorbed species aid in identification of reaction intermediates. Proton CRAMPS NMR has also been used to observe silanols and acid sites, but so far ^{1}H chemical-shift spectra have provided only qualitative information. We have found that NMR studies of deuterium-exchanged zeolites show dramatic differences between the various deuteron sites. ^{2}D spectroscopy of zeolites is a new technique that offers the potential to allow detailed, quantitative descriptions of Brønsted acid sites. Earlier studies have used deuterium spectra to assess adsorbate motion [4-7] or to detect deuterium exchange into acid sites [8], but both applications have been very qualitative treatments. During the past three years, we have conducted exploratory deuterium NMR studies of several zeolites, and we have examined acid sites alone and when interacting with basic probe molecules. Further studies are underway to determine the full range of capabilities of this new technique.

Deuterium NMR provides an alternative spectroscopic method for characterizing the environment of hydrogen in a material. Clearly, direct

observation of the acid center should be a sensitive measure of its properties. Deuterium magnetic resonance properties are quite different from those of hydrogen, in that the interaction of the deuteron quadrupole moment with the electric field gradient (EFG) at the nucleus dominates the spectrum. The resulting EFG information is interpreted much more readily than chemical-shift data. Depending on the sites involved, spectra may allow characterization of O-D bond strengths, bond lengths, or motion of bond axes. This work builds on the extensive use of deuteron NMR in polymers, where C-D bonds are well understood, and this technique has become a workhorse for elucidation of local motions in polymeric materials.

Experimental Methods

The zeolites used for the NMR studies were from the same batches of material used in other portions of this program. Samples of D-Y, D-ZSM-5, and D-mordenite were prepared with each of three deuteration techniques. In the first technique, sodium forms were exchanged to ND_4^+ forms by heating in ND_4NO_3/D_2O solutions, then heating to displace ND_3. In the second method, normal acid (H^+) forms were held at 373 K and exposed to 15 Torr D_2O vapor for several hours, which also produced deuterium exchange. Finally, adsorption and desorption of d_8-toluene were used to enrich exchangeable acid sites in deuterium.

NMR spectra were obtained on a Chemagnetics CMC-300A solid-state NMR spectrometer, operating at 46.0 MHz for ^2D. Pulses of 2.5-3.5 μs duration were used in the quadrupole echo sequence. T_1 and T_2 values were estimated from saturation-recovery and quad-echo experiments, respectively. Spectra shown here are typically accumulations of 500-1500 scans at 50 s recycle delay, depending on D enrichment, zeolite Al content, and T_1 values. Spectral fits were determined using a non-linear least-squares fitting routine. In principle, deuterium quadrupole spectra are symmetric about zero frequency; any asymmetries observable in these spectra are indicative only of non-ideal amplifier behavior.

Deuteron Site Identification

The spectrum of D-Y zeolite shown in Figure 11 contains two distinct species. This spectrum can be fit with a broad, two-horned Pake doublet and a narrower Gaussian line. The Pake doublet is indicative of an axially-symmetric environment and is typically seen for static deuterons in a well-defined environment. The quadrupole coupling constant (QCC) of 234 kHz is significantly smaller than the value of 320 kHz observed for O-D bonds in isolated D_2O molecules, indicating that the zeolitic O-D bond is weaker [9] and thus that this site has acidic character. The Gaussian line is similar in shape and width to the spectrum seen for D-exchanged surface silanol species on silica. Surface silanols and silanol nests in the zeolite would have a variety of environments and types of hydrogen-bonding to neighboring silanols. Both the distribution of sites and the possibility of motion (rotations or jumps between different H-bonded neighbors) contribute to the lack of discrete spectral features in this spectral component.

The acidic nature of these sites is seen in the effects of adsorption of basic molecules. Figure 12 shows the spectrum of the D-Y zeolite with NH_3 adsorbed. The new, narrow Lorentzian line is indicative of the formation of ammonium ions (NH_3D^+), with the rapid tumbling averaging the N-D bond EFG and producing a spectrum broadened only by the much smaller field gradients caused by the zeolite lattice. A fit to this spectrum indicates that all of the Pake doublet species and about half of the Gaussian species have been converted to ammonium ions, consistent with the above assignment of the doublet to Brønsted acid sites and the Gaussian to less acidic silanol species. When the sample is heated to desorb ammonia, the original sites are regenerated. The decrease in deuteration level is predicted well by considering the ammonia to remove 3/4 of the D from sites where ammonia has adsorbed.

Other zeolite frameworks produce different combinations of deuteration sites. Figure 13 shows spectra and fits for D-ZSM-5 and D-mordenite. For convenience, peaks will be labeled to indicate characteristic shapes and widths. In addition to the broad Pake doublet (α peak) and Gaussian (γ peak), the D-ZSM-5 spectrum contains a narrower Pake doublet (β peak) and a new powder pattern roughly half the width of the α peak that we have labelled the α' species. The D-mordenite spectrum contains the α' peak, a sharper β peak, a weak γ peak, and a narrow δ peak. The last feature is readily assigned to residual ammonium ions, since it resembles the peak seen in Figure 12, and also because it is difficult to remove all ammonium ions from mordenite. The other peaks are assigned to different Brønsted and silanol sites for the following reasons.

The γ peak indicates densely-packed surface silanols or silanol nests, as discussed earlier. The β peak may be generated from isolated silanol groups, which would be free to rotate about the Si-O axis. This free rotation produces a characteristic narrowing of the Pake doublet, with a reduced quadrupole coupling constant $QCC' = QCC_0 (3 \cos^2\theta - 1)/2$. If the static silanol O-D bond is comparable to that in water, using the water QCC of 320 kHz and the observed β peak QCC of 63 kHz, we calculate that the Si-O-D angle can be either 133±2° or 117±2°. The second of these two values compares nicely with the angle of 115±2° obtained from quantum calculations for this structure [10]. This assignment was tested by preparing two samples of the same Y zeolite, with the second heated under more demanding activation conditions to decrease the concentration of neighboring silanol groups via dehydration. As predicted, the first sample contained a significant γ peak, while the second sample had a reduced γ peak and observable intensity in the β peak. This result demonstrated that both peaks are caused by interconvertable silanol groups, either rotating freely in isolation or interacting with neighboring silanol groups. Further proof of this behavior was obtained by viewing the NMR spectra of silica samples. The spectrum of the fully hydrated sample was comprised of only a γ peak. As dehydroxylation proceeded, this peak decreased in intensity,

while the presence of a β peak became noticeable. However, at higher dehydration levels, a narrow Lorentzian peak, labeled the λ peak, also grew in intensity. The identity of the species responsible for this peak has not yet been ascertained.

The α peaks seen for D-Y and D-ZSM-5 indicate that these species are in axially-symmetric environments, as would be expected for rigid O-D bonds. These species have QCC's of 234 and 223 kHz, respectively, showing that the bond is significantly altered from the D_2O QCC of 320 kHz. Axial rotations seem unlikely, because of the large cone (25° half-angle) required to achieve this reduction. Instead, the EFG itself must be smaller because of either increased bond length, transfer of electrons to the O, or both. If the decrease is due solely to increased bond length, this would indicate an elongation from the normal O-D length of 0.96 Å to 1.07 Å. Such elongation could only be accompanied by a redistribution of electrons, so both effects are probably present and the actual bond lengthening would be less. A decrease in electron density and increase in bond length are consistent with weaker O-D bonding for this acidic species. This Brønsted site is thus clearly distinguished from a normal O-D species by its characteristic deuterium NMR spectrum.

The α' peaks seen for D-ZSM-5 and D-mordenite have QCC values near 120 kHz and asymmetry values (η) of 1. The indicated asymmetry of the electric field gradient cannot be obtained for an isolated O-D species or for any hydrogen-bonded species. However, such spectra are obtained by motional averaging between two sites at 109.4° from each other. This model also predicts that the apparent QCC decreases by a factor of 2, so this peak could be produced by two of the species generating the α peak exchanging and averaging with each other. A variety of other models have proved unsatisfactory for generating the α' peak. Since both the α and α' peaks can be rationalized using a single type of Brønsted site, with different motional properties, they have been assigned related labels. With this scheme, the D-Y zeolite sites experience little or no exchange, the D-mordenite is undergoing rapid exchange, and the D-ZSM-5 either has a single type of site with an intermediate exchange rate or two types of sites with fast and slow motions. These models make definite predictions about the temperature dependence of relative peak intensities for each sample, and further experiments are underway to test this theory.

This model for the α' peak also offers insight into the nature of the Brønsted site in a zeolite. Motional averaging could be considered between the different O atoms bonded to an Al center, or between different orientations on a single O atom. The jump angle is the tetrahedral angle for a 4-coordinated atom, leading to the picture that the deuteron may be hopping between the two lone pairs of an sp^3 O-atom bonded to neighboring Si and Al. This picture is in contrast to the widely-accepted structure, which has the H, Al, and Si atoms in the plane of an sp^2 O-atom [11, 12]. Such a structure could generate the α peak, but it could not alone give rise to the axially symmetric α' peak. Further consideration of known oxygen

chemistry also supports our assignment of this site as an sp^3 oxygen, since the only other sp^2 oxygens seen in bulk compounds have the remaining oxygen p orbital participating in a π bond. Finally, X-ray diffraction structural studies of the hydronium ion (H_3O^+) [13] show it to be pyramidal, with sp^3 hybridization rather than being a planar sp^2 species. Since this species and related oxonium ions are the closest known stable analogs to $SiAlOD^+$ Brønsted sites, this evidence supports our suggestion for reconsideration of the widely-accepted planar structure. This new structure will affect our understanding of Brønsted site location and accessibility, and it will also be critical for theoretical or computational modelling of zeolite properties.

Deuteron Site Interactions with Bases

We have conducted further experiments to examine reaction of D-Y, D-ZSM-5, and D-mordenite with ammonia and pyridine. All three zeolites have sharp Lorentzian lines for NH_3D^+ species. Pyridine produces characteristic triangular spectra, 160 kHz wide at the baseline. These spectra were comparable to spectra in the literature for deuterated aromatics adsorbed in H-form zeolites [14]. To produce this line shape, the deuteron transfers to the nitrogen and occupies an equatorial position on the rotating and wagging pyridinium ion.

The three deuterium exchange procedures also show the role of base strength in controlling selectivity of this process. Exchange using ND_4^+ was least selective, since the protons and deuterons in acid and silanol sites exchanged readily at the high temperatures used to desorb ammonia. Deuteration by adsorption of d_8-toluene and desorption by heating to 373 K was most selective for transfer of deuterons from the acidic toluene *para* or *ortho* positions to the Brønsted sites.

Further information on reactivities of different sites was obtained by sequential dosing experiments. Pyridine was first adsorbed on H-Y zeolite at a level sufficient to block part of the α peak or all of the γ peak. However, subsequent deuteration by D_2O vapor produced a spectrum with large γ peak intensity and approximately half the α peak intensity seen in Figure 11. This result is consistent with the assignment of the α peak to the Brønsted acid sites in the zeolite, since it is preferentially poisoned for D exchange by base adsorption.

Kinetic Studies of Methylamine Synthesis

Introduction

The synthesis of methylamines from methanol and ammonia over acid catalysts is of interest due to industrial demand and the need to develop catalysts selective to the lower substituted products. In addition, this reaction may be a useful probe of catalyst acidity. For example, in contrast to reactions such as hydrocarbon cracking, the products of methylamine synthesis consist of a limited number of molecules, and methylamine synthesis proceeds without catalyst deactivation over a wide variety of solid

acid catalysts. Accordingly, we have studied methylamine synthesis reactions at low conversions. In addition, we have studied the catalytic activities for the following related reactions: methylamine disproportionation reactions, reactions of methanol and dimethyl ether with methylamines, and methanol dehydration.

Experimental

A flow-through apparatus operating a 1 atm pressure was used for reaction kinetics measurements. An equimolar feed of NH_3 and CH_3OH was used for methylamine synthesis reaction studies, unless reaction orders or kinetics of related reactions were being studied. Analyses of the feed and reactor effluent streams were performed using a gas chromatograph with a packed column of 0.05 M/8% KOH washed Carbowax on Carbopack B.

The catalysts used in our kinetic studies are listed in Table 1. The acidities of the catalysts studied were assessed by microcalorimetric measurements of pyridine adsorption, and the results of these measurements are also provided in Table 1. Three NaH-Y zeolites (Linde) were studied with 33, 65, and 82 % of the Na exchange cations replaced by protons, and these catalysts are designated as NaH-Y-33, NaH-Y-65, and NaH-Y-82, respectively. The catalyst designated HYC was an H-Y zeolite-based fluid catalytic cracking catalyst obtained from R. Madon at Engelhard Corporation. The H-mordenite was obtained from Conteka Corporation. Three H-ZSM-5 catalysts were obtained from T. Degnan of Mobil Corporation (Paulsboro) with Si/Al ratios of 13, 27, and 225, and these samples are designated as H-ZSM-5-13, H-ZSM-5-27, and H-ZSM-5-225, respectively. Another H-ZSM-5 catalyst, designated as H-ZSM-5-35, had a Si/Al ratio of 35 and was provided by W. Haag of Mobil Corporation (Princeton). The amorphous silica-alumina designated SAC was obtained from Davison Corporation and had an aluminum loading of 13 wt%. The silica catalyst was a fumed silica grade EH-5 obtained from Cabot Corporation.

Methylamine Synthesis Reactions

Catalytic activities and apparent activation energies were determined for all catalysts, and reaction orders in ammonia and methanol were measured for selected samples. Silica did not show measurable activity for either methylamine synthesis or methanol dehydration to dimethyl ether (DME) at temperatures up to 673 K.

Apparent activation energies were measured for production of each of the methylamines and DME. Figure 14 shows Arrhenius plots for total methylamines synthesis for a sampling of the catalysts. The rate of DME production was generally of the same order of magnitude as the total methylamines production rate for all catalysts. Examples of Arrhenius plots for DME production appear in Figure 15.

Table 2 summarizes the activation energies for production of the individual products for the different catalysts. The apparent activation energy for total amine formation varies from 14 to 29 kcal/mol, with an average value of 19 kcal/mol. For all catalysts, the activation energy for trimethylamine formation was highest, while that for monomethylamine

the lowest. This trend was observed for SAC, HYC, H-ZSM-5-35, and H-mordenite, reflecting little influence of catalyst morphology. DME formation proceeds with an apparent activation energy in the range from 3 to 25 kcal/mol, with an average value of 16 kcal/mol.

Turnover frequencies for total amine formation during methylamine synthesis were calculated, assuming that the active sites for each catalyst were sites on which the heat of pyridine adsorption was greater than that for hydrogen bonding to non-acidic hydroxyl groups (greater than 95-110 kJ/mol). These results are shown in Table 3. An interesting feature of these data is that the turnover frequencies for these catalysts fall within a relatively narrow range. The fact that a variety of zeolitic structures and amorphous silica-alumina are represented in this table indicates that structural considerations do not have a major effect on activity of the samples studied at low conversions.

The dependence of methylamine formation at 603 K on ammonia partial pressure is shown in Figure 16. Methylamine production was first order in ammonia for the NaHY-82, H-mordenite, H-ZSM-5-35, and silica-alumina catalysts studied.

DME production over NaHY-82, H-mordenite, H-ZSM-5-35, and silica-alumina catalysts was inhibited by increasing ammonia partial pressures. Figure 17 shows examples of this behavior.

Methylamine formation at 603 K over HYC, H-mordenite, and silica-alumina catalysts was positive order in methanol at low pressures but zero order at higher pressures. These results are shown in Figure 18. The H-ZSM-5 catalysts demonstrate negative reaction order in methanol at high pressures. DME production was generally first order in methanol for all catalysts.

Methylamine Disproportionation Reactions

Kinetic studies were undertaken of methylamine disproportionation reactions over H-ZSM-5-35, since reactions of this type may be important during methylamine synthesis from methanol and ammonia. Figure 19 shows the results obtained when monomethylamine (MMA) was passed over H-ZSM-5-35 at a pressure of 2.6 Torr and various temperatures. The primary products of MMA disproportionation are NH_3 and dimethylamine (DMA). However, the results show that DMA can further disproportionate to trimethylamine (TMA) and MMA. The disproportionation of MMA is rapid compared to the reaction between ammonia and methanol to form methylamines. For example, at 623 K, the rate of disproportionation is approximately 10 times faster than that of total amine production under comparable conditions.

The results of DMA disproportionation studies at a partial pressure of DMA equal to 1.1 Torr show that MMA and TMA are the predominant products, with small amounts of NH_3 formed via secondary disproportionation. The rate of DMA disproportionation at 623 K is approximately twice as fast as MMA disproportionation and 20 times faster than amine formation from methanol and ammonia.

Reactions of Methylamines with Methanol

Reactions of methanol with MMA and DMA were studied to evaluate the relative rates of disproportionation and series methylation processes. Reaction conditions were identical to those used for methylamine disproportionation studies, except for the addition of methanol at 7 Torr.

The addition of methanol to the MMA feed over H-ZSM-5-35 reduces the amount of NH_3 observed, most likely due to reaction between NH_3 and CH_3OH to form MMA. The rate of DMA production remains essentially unchanged with CH_3OH addition, but there is a slight increase in the rate of TMA formation.

The effects of methanol addition to DMA are similar to the behavior observed for MMA disproportionation. Specifically, methanol addition leads to a threefold decrease in the amount of MMA formed from DMA, while the rate of TMA formation remains essentially unchanged upon addition of methanol to DMA.

Methanol Dehydration

The dehydration of methanol to form DME was studied at 603 K by flowing CH_3OH at 4-28 Torr over H-ZSM-5-35. The reaction appears to be second order with respect to methanol pressure. Furthermore, the rate of DME formation with methanol is approximately 20 times faster than that under methylamine synthesis conditions, i.e., in mixtures of methanol and ammonia.

Adsorption of Reactants/Products of Methylamine Synthesis

Experimental

Two of the above catalysts employed in our kinetic studies were also used for calorimetric adsorption studies: H-ZSM-5 and H-mordenite. The calorimeter temperature was typically 473 K for these experiments. The following molecules were used in this series of adsorption studies: ammonia, monomethylamine, dimethylamine, trimethylamine, methanol, dimethyl ether, and water. Co-adsorption experiments were also conducted, in which methanol or DME was first adsorbed on H-mordenite at 473 K, followed by ammonia adsorption at 473 K.

Infrared spectra were recorded using a Nicolet model 7199C Fourier transform infrared spectrometer. Methanol, ammonia, and monomethylamine were used in these adsorption studies. Each molecule was allowed to adsorb at room temperature. Helium was then flowed at 100 cm^3/s through the treatment cell, and spectra were taken after the initial helium purge at room temperature and at various temperatures up to typically 623 K. In-situ reaction studies were also performed with the H-ZSM-5 catalyst under partial pressures of 10 Torr CH_3OH, 7 Torr NH_3, and 743 Torr He.

Microcalorimetric Adsorption Studies

The differential heat of adsorption versus coverage for ammonia on H-ZSM-5 was shown earlier in Figure 4. There are two plateaus corresponding to adsorption on strong and weak sites. The strong sites have

an average heat of adsorption of 149 ± 10 kJ/mol. The weak sites adsorb ammonia at 69 ± 4 kJ/mol. There are approximately 300 μmol/g of strong sites. Infrared spectroscopy shows that these sites are Brønsted acid centers. The behavior for ammonia adsorption on H-mordenite is similar to that on H-ZSM-5. The major difference between these two samples is that mordenite also has a few very strong sites in addition to the large number of strong sites. We have also observed the very strong sites for pyridine adsorption on H-mordenite. The total number of strong adsorption sites is approximately 900 μmol/g, with an average heat of ammonia adsorption of 157 ± 8 kJ/mol. The weak sites adsorb ammonia at 72 ± 2 kJ/mol.

Figure 20 shows the differential heat plot for monomethylamine adsorption on H-ZSM-5. The heat of adsorption gradually decreases from 230 to 180 kJ/mol as the coverage increases to 300 μmol/g. The average heat of adsorption for these sites is 210 ± 11 kJ/mol. Weak sites of MMA adsorption strength equal to 102 ± 4 kJ/mol are titrated between 330 and 350 μmol/g. However, at higher coverages a higher heat is observed, probably due to bimolecular reactions between amine molecules. MMA adsorption on H-mordenite also shows a plateau corresponding to sites with heats that decrease monotonically with increasing coverage. At high coverages, an apparent increase in heat with each dose is also observed. The number of sites titrated by MMA for H-mordenite is lower than the number titrated by ammonia, approximately 520 μmol/g. The average heat of adsorption for the strong sites is 219 ± 10 kJ/mol, and for the weak sites the corresponding value is 97 ± 6 kJ/mol.

The differential heat of DMA adsorption on H-ZSM-5 is essentially constant at 250 ± 10 kJ/mol with increasing coverage, and it decreases to 135 ± 10 kJ/mol at high coverages. The differential heat curve for DMA adsorption on H-mordenite shows a gradually decreasing heat of adsorption followed by titration of weak sites. As for MMA adsorption, high heats are observed at high coverages probably due to reactions between amine molecules. The average heats of DMA adsorption on these sites are 212 ± 7 and 134 ± 6 kJ/mol respectively.

TMA adsorption on H-ZSM-5 shows a gradually sloping differential heat curve. The average heat of adsorption for the first 200 μmol/g of sites titrated is 154 ± 4 kJ/mol. The heat of adsorption for the strongest sites is lower than that for MMA and DMA. This behavior is surprising given that TMA has the highest proton affinity of the methylamines. The adsorption behavior of TMA on H-mordenite is similar to that for TMA adsorption on H-ZSM-5. Instead of well-defined plateaus, the differential heat of adsorption steadily decreases with increasing coverage. At a coverage of approximately 700 μmol/g, the heat decreases more rapidly. The average strength of TMA adsorption on sites up to this coverage is 143 ± 4 kJ/mol. As with adsorption on H-ZSM-5, the heat of TMA adsorption on H-mordenite is lower than that for MMA or DMA.

Figure 8 showed earlier the differential heat plot for dimethyl ether adsorption on H-ZSM-5. Some sites apparently have very high strength, whereas a large number of sites have an intermediate heat of 96 ± 3 kJ/mol. Weak sites also exist with an average heat of DME adsorption equal to 44 ± 2 kJ/mol. Approximately 320 μmol/g of strong sites are titrated by DME. We

have also measured the differential heat of adsorption of DME on H-mordenite at 373 K. There is an initial region of high-strength adsorption, followed by adsorption on sites with a heat equal to 87 ± 4 kJ/mol. The heat of adsorption decreases gradually with coverage to 60 kJ/mol. The adsorption of DME titrates strong sites up to a coverage of 750 μmol/g on H-mordenite.

The differential heat of methanol adsorption on H-ZSM-5 at 373 K indicates that the strong sites adsorb CH_3OH at 80 ± 3 kJ/mol, while the weak sites give a heat of adsorption near 66 ± 3 kJ/mol. The heats of methanol adsorption on strong and weak sites of H-mordenite are equal to 100 ± 4 and 71 ± 3 kJ/mol, respectively.

The differential heat of adsorption of water on H-ZSM-5 at 373 K shows one discernable plateau, with an average heat of adsorption of 61 ± 2 kJ/mol. The differential heat curve for water adsorption on H-mordenite at 423 K shows an initial decrease in heat of adsorption, followed by a long plateau, with an average heat of adsorption equal to 75 ± 2 kJ/mol.

Ammonia adsorption was studied on H-mordenite following treatment with methanol. In particular, methanol adsorption at 473 K was continued to an equilibrium pressure of 5 Torr, and gaseous methanol was then evacuated. The catalyst temperature was raised to 523 K, and the catalyst degassed overnight at a pressure of 10^{-5} Torr. Ammonia adsorption was then conducted at 473 K. Methanol preadsorption followed by evacuation has the effect of reducing the number of strong adsorption sites. The heat of adsorption on the remaining Brønsted sites is not affected by the irreversibly bound methanol species. The effect on ammonia adsorption of DME preadsorption was similar to that found for methanol preadsorption.

Infrared Spectroscopy

Ammonia was adsorbed at room temperature on H-ZSM-5 at a pressure of 7 Torr. The IR bands due to silanol and acidic hydroxyl groups are eliminated with room temperature ammonia adsorption. Increasing the desorption temperature led first to ammonia desorption from the silanol groups, with essentially complete desorption by 573 K. Ammonia bound to Brønsted hydroxyls began to desorb at 573 K. The corresponding spectra for the N-H vibration regions are shown in Figure 21. Following adsorption at room temperature, and with residual ammonia in the gas phase, there is a broad band between 3400 and 2800 cm^{-1} corresponding to weakly adsorbed ammonia, as well as strong bands at 1621 and 1493 cm^{-1}. The band at 1493 cm^{-1} corresponds to ammonium ions due to ammonia associated with a Brønsted acid sites, while that at 1621 cm^{-1} is most likely due to interaction of ammonia with residual Na^+. As gas-phase ammonia is purged and the catalyst temperature raised to 373 K, the bands due to weakly held ammonia disappear. With increasing temperature from 473 K to 623 K, the band due to ammonia adsorbed on Brønsted sites decreases in intensity.

Monomethylamine was adsorbed on H-ZSM-5 at a pressure of approximately 40 Torr. The general behavior was similar to that for ammonia adsorption, except that the hydroxyl band due to Brønsted sites was not recovered, even at 673 K. This behavior is consistent with the fact

that MMA adsorbs more strongly than NH_3. Figure 22 shows the infrared spectra in the region of MMA absorbance after MMA adsorption at room temperature and after purging in flowing He at room temperature and at increasing temperatures. Weakly adsorbed MMA gives rise to a broad series of bands in the range 3200 - 2600 cm^{-1}. The strong bands at 1597 and 1464 cm^{-1} are the asymmetric and symmetric vibrations of MMA adsorbed on Brønsted acid sites. The presence of these two bands at high temperatures indicates that adsorption of MMA is strong on the Brønsted acid sites.

Figure 23 shows spectra for H-ZSM-5 with methanol adsorbed at 7 Torr and 298 K, after initiating a flow of He at 298 K and raising the catalyst temperature. Room-temperature adsorption of methanol results in a broad band with peaks at 2949 and 2842 cm^{-1} and shoulders at 2989 and 2922 cm^{-1}. These peaks in the 2900-2800 cm^{-1} region are due to the O-H stretch of hydrogen-bound methanol. Purging with He and raising the temperature to 523 K results in the elimination of all bands but those at 2957 and 2856 cm^{-1}. The sharp peak at 2856 cm^{-1} is assigned to the symmetric CH_3 vibration of methoxy groups resulting from methyl substitution at Brønsted acid sites; the accompanying broad band at 2957 cm^{-1} is the corresponding asymmetric CH_3 vibration.

Figure 24 shows IR spectra of H-ZSM-5 collected under methylamine reaction conditions. The bands at 2922 and 2989 cm^{-1} disappear at temperatures above 373 K, leaving only the pair of methoxy bands at 2957 and 2855 cm^{-1}. The region of amine absorbance under reaction conditions is shown in Figure 25. The peak centered at 1469 cm^{-1} is most likely due to ammonia adsorbed on Brønsted sites. A second small peak at 1625 cm^{-1} can be assigned to ammonia adsorbed at Na^+ cations. Increasing the reaction temperature to 523 K results in decreasing amounts of adsorbed ammonia. At 573 K, two new peaks appear, centered at 1611 and 1465 cm^{-1}. These bands can be assigned to MMA.

Implications of Results

Table 4 summarizes the proton affinities and the heat of adsorption data for the reactants and products in methylamine synthesis. Molecules with a higher proton affinity have higher heats of adsorption. Trimethylamine is a notable exception, and this result may be due to steric effects. Ammonia has a higher heat of adsorption than methanol and would be expected to be the dominant species adsorbed on the Brønsted acid sites in the presence of these two gases. Monomethylamine, the primary reaction product at low conversion, has a higher heat of adsorption than ammonia, and MMA might, therefore, be expected to occupy a significant fraction of the adsorption sites under reaction conditions. The infrared spectroscopy results for NH_3 and MMA confirm that these molecules coordinate with the Brønsted acid sites, and spectra at increasing desorption temperatures are consistent with the measured strengths of adsorption on the hydrogen-bonding and Brønsted sites of H-ZSM-5.

Methanol can coordinate with Brønsted acid sites and also transform Brønsted hydroxyl groups into methoxy groups. DME can also form

methoxy species. An important result revealed by the coadsorption experiments is that methoxy groups can act only as weak adsorption sites for amines. The in-situ infrared spectroscopy results of this study are consistent with the idea that methoxy groups may be important species in methylamine synthesis, either as active species or as species that block acid sites. Under reaction conditions, even at temperatures up to 673 K, methoxy groups can be observed on the catalyst surface. The *in situ* IR experiments also suggest that ammonia coverage is low on the catalyst surface during reaction. In contrast, MMA coverage increases as temperature increases from 573 K to 673 K. This is the temperature range in which the rate of methylamine synthesis becomes significant. The *in situ* IR studies thus show that the Brønsted acid sites become largely covered by methylamines and methoxy species under reaction conditions.

Catalytic Cycles for Methylamine Synthesis

General Aspects of Reaction Kinetics

Our kinetic studies of methylamine synthesis show that the methylamine formation rate is first order with respect to the ammonia pressure for reaction temperatures from 603 K to 723 K. This dependence of rate on ammonia pressure suggests that the surface coverage of ammonia is low. As shown above, the ammonia adsorption sites may be primarily covered with methylamines, which adsorb more strongly than ammonia.

For all of the catalysts studied, the rate of DME formation is inversely proportional to ammonia partial pressure. This behavior indicates that ammonia blocks surface species involved in DME formation. Methoxy species are probable surface intermediates involved in methanol dehydration to DME, and these species are apparently blocked by adsorbed ammonia or amines.

An important result of this study is that the dependence of the methylamine synthesis rate on the methanol pressure is rather complex. Based on adsorption thermodynamics alone, the surface coverage of adsorbed methanol on the acid sites is expected to be low in comparison with the strongly basic amines. The observed methanol dependence of the rate must, therefore, be kinetically rather than thermodynamically controlled.

Disproportionation of MMA and DMA is faster than the rate of MMA formation from methanol and ammonia. The fact that TMA is readily formed from DMA on H-ZSM-5-35 demonstrates that the pore structure of H-ZSM-5 does not limit TMA formation. Since MMA formation can be observed without detection of DMA under methylamine synthesis conditions, we conclude that the disproportionation pathways are slower under methylamine synthesis conditions, due to the presence of surface species (e.g., methoxy species) formed from methanol or due to the fact that the pressures of MMA and DMA are higher under the amine disproportionation reaction conditions employed in our studies.

The rate of methanol conversion to dimethyl ether is significantly slower in the presence of ammonia or other amines. Accordingly, this reaction pathway is suppressed under methylamine synthesis reaction conditions. This behavior is further evidence that methanol dehydration

takes place through an intermediate (e.g., methoxy species) that is blocked by adsorbed ammonia and amines.

Formulation of Catalytic Cycles

Infrared spectroscopy studies give clear evidence for the presence of methoxy species on H-ZSM-5-35 in flowing methanol. These species are also present in smaller amounts under reaction conditions for methylamine synthesis. We suggest that methoxy species are reactive intermediates in the dehydration of methanol to DME. Indeed, there is considerable literature evidence for alkoxy species being important for carbenium ion chemistry and as intermediates in DME formation e.g., [15-18] It is less clear whether these species are involved in the synthesis of methylamines from methanol and ammonia.

The calorimetric studies show that in addition to acid sites, all catalysts possess non-acidic sites on which the reactants and products of this study adsorb with strengths ranging from about 50-140 kJ/mol. These sites may be associated with hydrogen bonding or non-specific interactions within the catalyst micropores (e.g., van der Waals interactions, polarization effects).

We now present a general sequence of steps that describes the essential aspects of methylamine synthesis and related catalytic processes. The first steps in the sequence are adsorption and desorption of all reactants and products onto the weak, non-acidic sites of the catalyst, represented by #:

1. $CH_3OH + \# \Leftrightarrow CH_3OH\#$
2. $H_2O + \# \Leftrightarrow H_2O\#$
3. $DME + \# \Leftrightarrow DME\#$
4. $NH_3 + \# \Leftrightarrow NH_3\#$
5. $MMA + \# \Leftrightarrow MMA\#$
6. $DMA + \# \Leftrightarrow DMA\#$
7. $TMA + \# \Leftrightarrow TMA\#$

These steps are followed by migration of weakly adsorbed species on #-sites to acid sites, represented for simplicity as Brønsted acid sites OH*:

8. $NH_3\# + OH^* \Leftrightarrow NH_4O^* + \#$
9. $MMA\# + OH^* \Leftrightarrow HMMAO^* + \#$
10. $DMA\# + OH^* \Leftrightarrow HDMAO^* + \#$
11. $TMA\# + OH^* \Leftrightarrow HTMAO^* + \#$

The adsorption of methanol, water, and DME onto the acid sites has not been included because the interactions of these molecules with acid sites are weak. (We note that all of the catalysts studied in our work show primarily Brønsted acidity, and as such we have no information regarding the possible catalytic properties of Lewis acid sites.)

The dehydration of methanol to DME can be represented by adding the following two reaction steps involving methoxy species:

12. $CH_3OH\# + OH^* \Leftrightarrow CH_3O^* + H_2O\#$
13. $CH_3OH\# + CH_3O^* \Leftrightarrow OH^* + DME\#$

The catalytic cycle for methanol dehydration thus consists of Steps 1,2,3,12, and 13. This reaction can exhibit first- or second-order kinetics with respect to methanol pressure, depending on whether the surface methoxy coverage is zero or first order with respect to methanol. Also, this reaction will be suppressed in the presence of ammonia or amines, since these nitrogen-bases interact more strongly with acid sites than do methoxy species.

Methylamine synthesis and disproportionation reactions can be written with or without participation of methoxy species. Consider, for example, the following steps:

14. $NH_3\# + CH_3O^* \Leftrightarrow HMMA^* + \#$
15. $MMA\# + CH_3O^* \Leftrightarrow HDMA^* + \#$
16. $DMA\# + CH_3O^* \Leftrightarrow HTMA^* + \#$

The catalytic cycle for MMA disportionation is comprised of Steps 4,5,6,8,9,10,14, and 15. The difficulty with this cycle is that it cannot predict the observed effect of adding methanol to MMA, i.e., the suppression of ammonia formation. In particular, the $NH_3\#$ produced in the reverse of Step 14 cannot readsorb on acid sites because these sites are covered by strongly adsorbed MMA species. Therefore, methanol reacts with methoxy species in Step 13 to form DME. In contrast to this predicted behavior, the experimental data show that DME is not produced when methanol and MMA are passed over H-ZSM-5.

To solve this problem, consider the following steps for methylamine disproportionation reactions involving reactions between weakly and strongly adsorbed species:

17. $HMMAO\# + HMMAO^* \Leftrightarrow NH_4O\# + HDMAO^*$
18. $HMMAO\# + HMMAO^* \Leftrightarrow NH_4O^* + HDMAO\#$
19. $HDMAO\# + HDMAO^* \Leftrightarrow HMMAO\# + HTMAO^*$
20. $HDMAO\# + HDMAO^* \Leftrightarrow HMMAO^* + HTMAO\#$

The physical basis for using steps such as 17 and 18 is that the quaternary amine species associated with the acid sites may rotate on the surface such that disproportionation of these species with weakly adsorbed amine species may lead to either of the reaction products becoming associated with the acid site. The reaction scheme represented by Steps 17-20 is also consistent with the experimental result that the rates of MMA and DMA disproportionation are an order of magnitude higher than the rates of methylamine synthesis from methanol and ammonia. In particular, the pressures of MMA and DMA under the methylamine synthesis conditions of this study are at least an order of magnitude lower than the pressures of MMA and DMA employed for studies of disproportionation reactions. While the surface coverages by strongly adsorbed HMMAO* and HDMAO* are not sensitive to the MMA and DMA pressures, the surface coverages by weakly adsorbed MMA# and DMA# are directly proportional to pressure; therefore, the reaction scheme represented by Steps 17-20 gives the proper dependence of the disproportionation rate on pressure. Finally, Steps 17-20 also give the proper rate of disproportionation when employing reasonable values of preexponential factors.

The reaction steps (replacing Steps 14-16) leading to methylamine synthesis and to the effects of adding methanol to MMA and DMA may be rewritten as:

21. $CH_3OH\# + NH_4O^* \Leftrightarrow HMMAO^* + H_2O\#$

22. $CH_3OH\# + HMMAO^* \Leftrightarrow HDMAO^* + H_2O\#$

23. $CH_3OH\# + HDMAO^* \Leftrightarrow HTMAO^* + H_2O\#$

The proposed catalytic cycle represented by Steps 1-13 and 17-23 is an attempt to capture in a consistent fashion the catalytic chemistry of the methylamine synthesis and related reactions. Major points that must be satisfied by this catalytic cycle are that methylamine synthesis involves the formation and participation of very strongly adsorbed species, and the rate of methylamine synthesis is a rather complex function of the methanol pressure.

In the absence of weak sites, methylamine species must desorb directly from the acid sites to the gas phase. Since the heats of adsorption of MMA and DMA are at least 200 kJ/mol, the maximum rates of desorption are equal to 10^{-5} sec^{-1} at 623 K, assuming a normal value of the desorption preexponential factor equal to 10^{13} sec^{-1}. This maximum rate is several orders of magnitude lower than the observed rate of methylamine disproportionation. Furthermore, the activation energies of methylamine synthesis and related reactions are significantly lower than the heats of MMA or DMA adsorption on the acid sites. However, the desorption of strongly adsorbed MMA and DMA onto weaker sites is much faster (e.g., 10^4 sec^{-1}), and high turnover frequencies for MMA and DMA disporportionation can be achieved. Accordingly, we reach the important conclusion that acid sites, as well as weak adsorption sites, are critical for methylamine synthesis and related reactions, i.e., acid sites are required for the critical reaction steps and weak sites are required to facilitate desorption of strongly adsorbed amines from the acid sites and for disproportionation.

The complex reaction kinetics of methylamine synthesis with respect to the methanol pressure can be explained by the proposed catalytic cycle in terms of the surface coverage by CH_3O^*. For example, while these species are involved in DME formation from methanol, surface methoxy species are not apparently involved in methylamine synthesis or disproportionation steps, and higher surface coverages by these species lead to lower coverages of reactive amine species on the acid sites. Furthermore, DME formation under methylamine synthesis reaction conditions is not inhibited by methanol, and this observed behavior is consistent with the suggestion that methoxy species are reactive intermediates for this reaction.

References

1. Deeba, M., in "Acidity Distribution on Oxide Surface", PhD Thesis, University of Wisconsin-Milwaukee, (1978).

2. Deeba, M. and Hall, W.K., *Z. Phys. Chem. Neue Folge*, **144**, 85, (1985).

3. Benson, J.E., Ushira, K., and Boudart, M., *J. Catal.*, **9**, 91, (1967).

4. Eckman, R.E. and Vega, A.J., *J. Phys. Chem.*, **90**, 4679, (1986).

5. Luz, Z. and Vega, A.J., *J. Phys. Chem.*, **90**, 4903, (1986).

6. Silbernagel, B.G., Garcia, A.R., Newsam, J.M., and Hulme, R., *J. Phys. Chem.*, **96**, 2629, (1992).

7. Hepp, M.A., Ramamurthy, V., Corbin, D.R., and Dybowski, C., *J. Phys. Chem.*, **96**, 2629, (1992).

8. Vega, A.J. and Luz, Z., *J. Phys. Chem.*, **91**, 365, (1987).

9. Rinné, M. and Depireux, J., *Adv. Nucl. Quad. Reson.*, **1**, 357, (1974).

10. Mortier, W.J., Sauer, J., Lercher, J.A., and Noller, H., *J. Phys. Chem.*, **88**, 905, (1984).

11. Olson, D.H. and Dempsey, E., *J. Catal.*, **13**, 221, (1969).

12. Jirák, Z., Vratislav, S., Zajícek, J., and Bosácek, V., *J. Catal.*, **49**, 112, (1977).

13. Lundgren, J.O. and Williams, J.M., *J. Chem. Phys.*, **58**, 788, (1973).

14. Kustanovich, I., Vieth, H.M., Luz, Z., and Vega, S., *J. Phys. Chem.*, **93**, 7427, (1989).

15. Parera, J. and Figoli, N., *J. Catal.*, **14**, 303, (1969).

16. Detrekoy, E. and Kallo, D., *Acta. Chim. Acad. Sci. (Hungary)*, **95**, 201, (1977).

17. Matsushima, T. and White, J., *J. Catal.*, **44**, 183, (1976).

18. Kramer, G.M., McVicker, G.B., and Ziemiak, J.J., *J. Catal.*, **92**, 355, (1985).

Tables

Table 1. Catalyst Properties

Sample	Acid Site Density (μmol/g)	Average Brønsted site strength (kJ/mol for pyridine adsorption)
NaHY-82	1450	138
NaHY-65	1000	152
NaHY-33	360	146
HYC	180 Brønsted/308 total	165
H-mordenite	710	204
H-ZSM-5-13	670	181.6
H-ZSM-5-27	603 (estimated)	not measured
H-ZSM-5-225	74 (estimated)	not measured
H-ZSM-5-35	360	181
SAC	90 Brønsted/204 total	146

Table 2. Summary of Apparent Activation Energies

Sample	Activation Energies				
	Total Amines	MMA	DMA	TMA	DME
NaHY-82	25.74	17.06	24.24	43.11	17.10
NaHY-65	21.53	10.40	24.63	39.35	11.90
NaHY-33	12.39	11.01			18.22
HYC	18.96	13.39	24.22	37.55	21.89
H-mordenite	17.13	15.53	23.79	26.24	2.91
H-ZSM-5-13	15.89	13.77	21.32	37.24	15.36
H-ZSM-5-27	20.90	18.35	22.09	35.67	9.21
H-ZSM-5-225	16.54	15.97			24.29
H-ZSM-5-35	14.43	14.04	18.10	38.42	12.74
SAC	20.23	12.97	21.53	33.97	12.75
Average	18.80	15.29	20.61	33.63	13.82

Table 3 Methylamine Synthesis Turnover Frequencies at 667 K

Sample	Turnover Frequency ($ksec^{-1}$)
NaHY-82	2.3
NaHY-65	0.5
NaHY-33	0.1
HYC	1.1
H-mordenite	2.1
H-ZSM-5-13	1.1
H-ZSM-5-27	0.8
H-ZSM-5-225	0.1
H-ZSM-5-35	1.6
SAC	4.1

Table 4. Average heats of adsorption on H-ZSM-5 and H-mordenite

Base	Proton Affinity PA (kJ/mol)	H-ZSM-5		H-mordenite	
		ΔH_1 (kJ/mol)	ΔH_2 (kJ/mol)	ΔH_1 (kJ/mol)	ΔH_2 (kJ/mol)
NH_3	857.7	149 ± 11	69 ± 4	157 ± 8	72 ± 2
NH_2CH_3	895.8	219 ± 11	102 ± 4	219 ± 10	97 ± 6
$NH(CH_3)_2$	922.6	250 ± 10	143 ± 8	212 ± 7	134 ± 6
$N(CH_3)_3$	938.5	154 ± 4	65 *	143 ± 4	66 *
CH_3OH	773.6	80. ± 3	66 ± 3	100 ± 4	71 ± 2
CH_3OCH_3	807.9	96 ± 3	44 ± 2	87 ± 4	61 *
H_2O	723.8	61 ± 3		75 ± 2	

* denotes lowest measured value
ΔH_1 = high strength adsorption sites
ΔH_2 = low strength adsorption sites

Figures

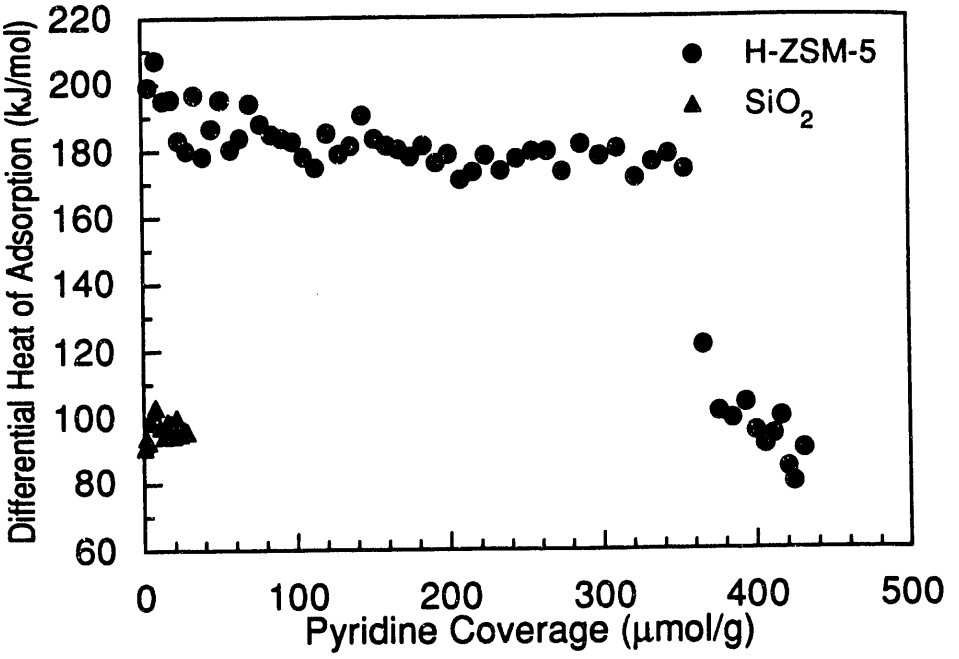

Figure 1. Differential heat of pyridine adsorption versus pyridine coverage on H-ZSM-5 at 473 K.

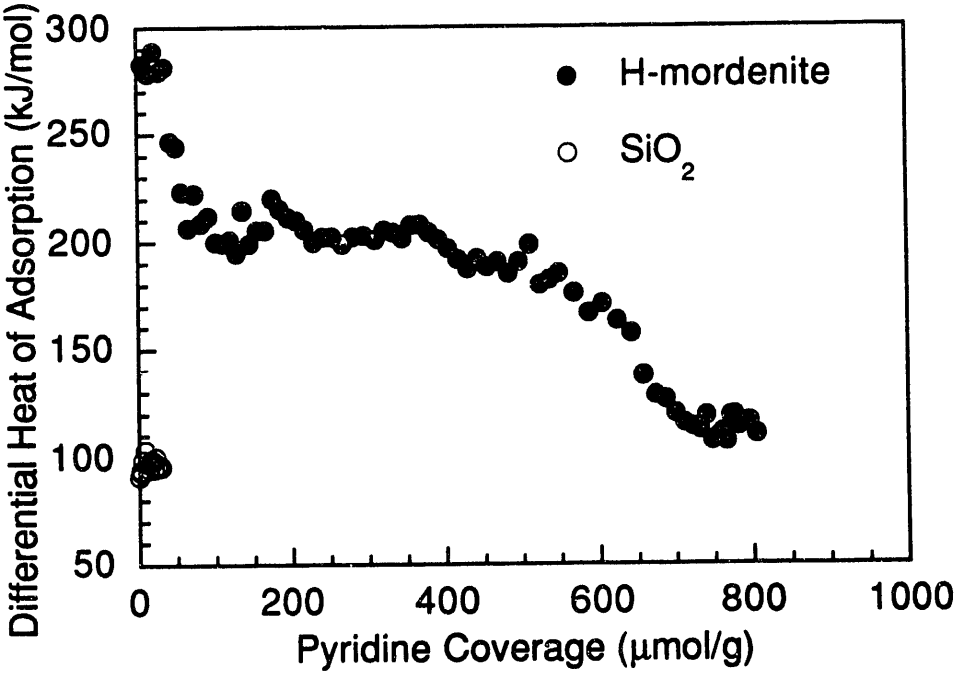

Figure 2. Differential heat of pyridine adsorption versus pyridine coverage on H-mordenite at 473 K.

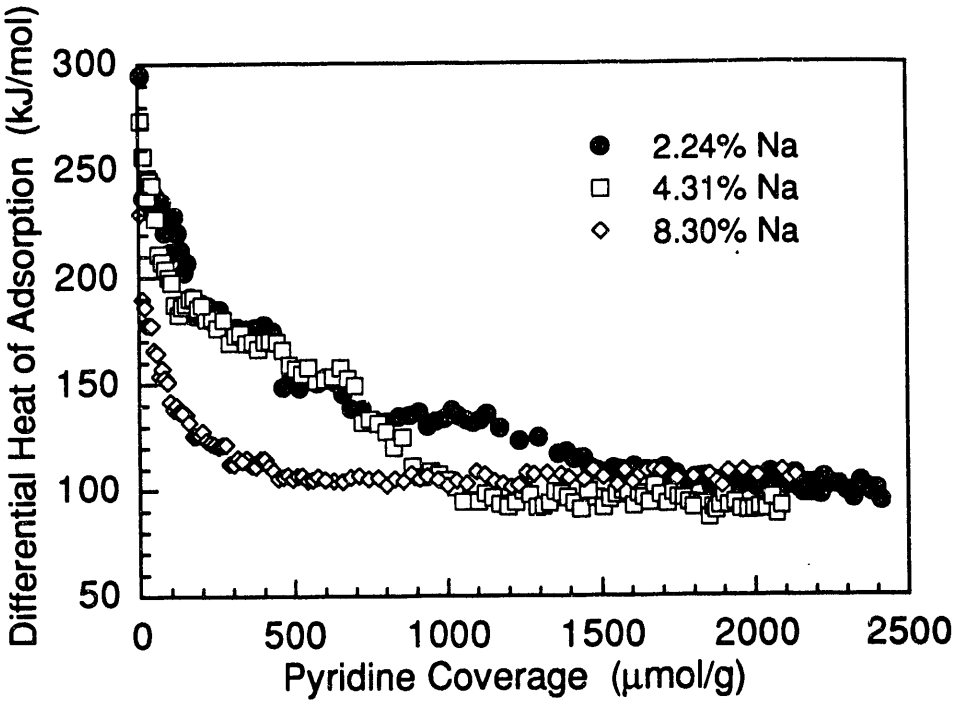

Figure 3. Differential heat of pyridine adsorption versus pyridine coverage on HNa-Y zeolite at 473 K with 33, 65, and 82% of the Na exchange cations replaced by protons.

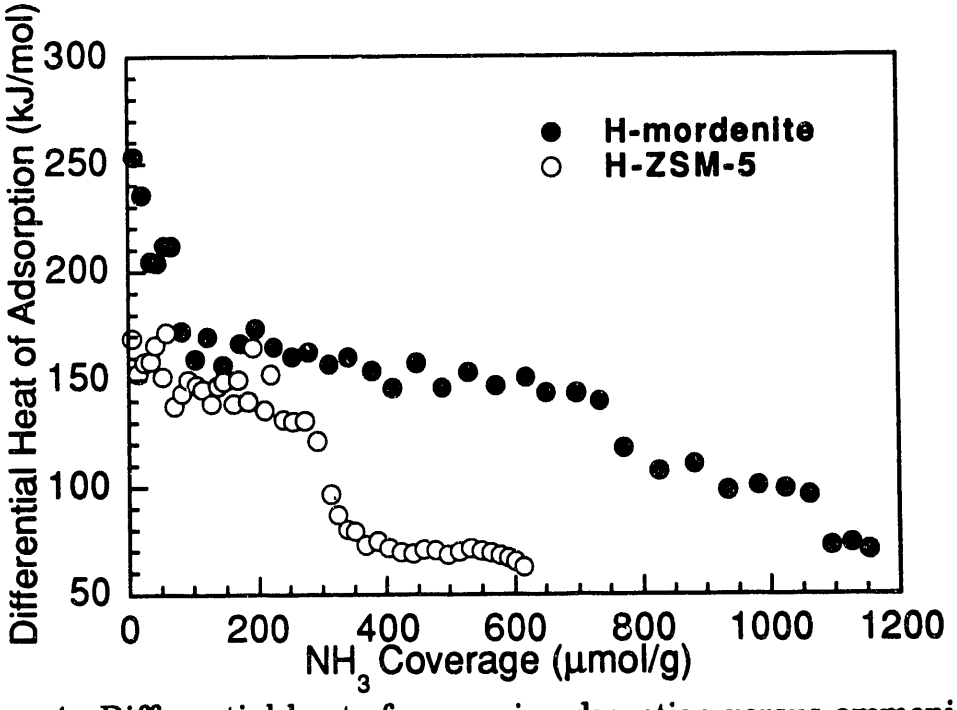

Figure 4. Differential heat of ammonia adsorption versus ammonia coverage on H-ZSM-5 (•) and H-mordenite (o) at 473 K.

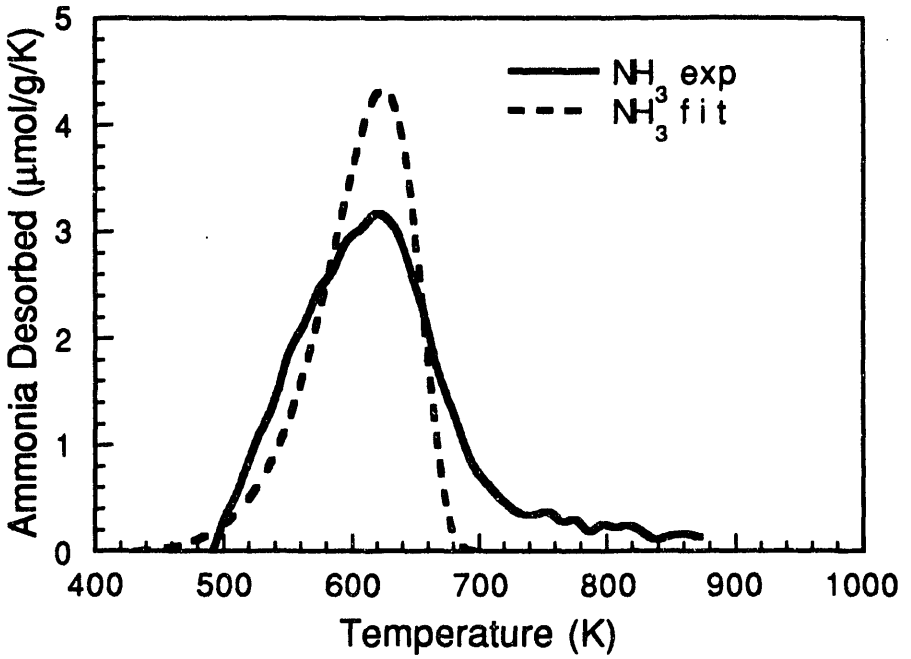

Figure 5. Temperature-programmed desorption results for ammonia from H-ZSM-5. Solid curve is the experimental spectrum and the dashed curve is a computer simulation. (Heating rate = 10 K/min)

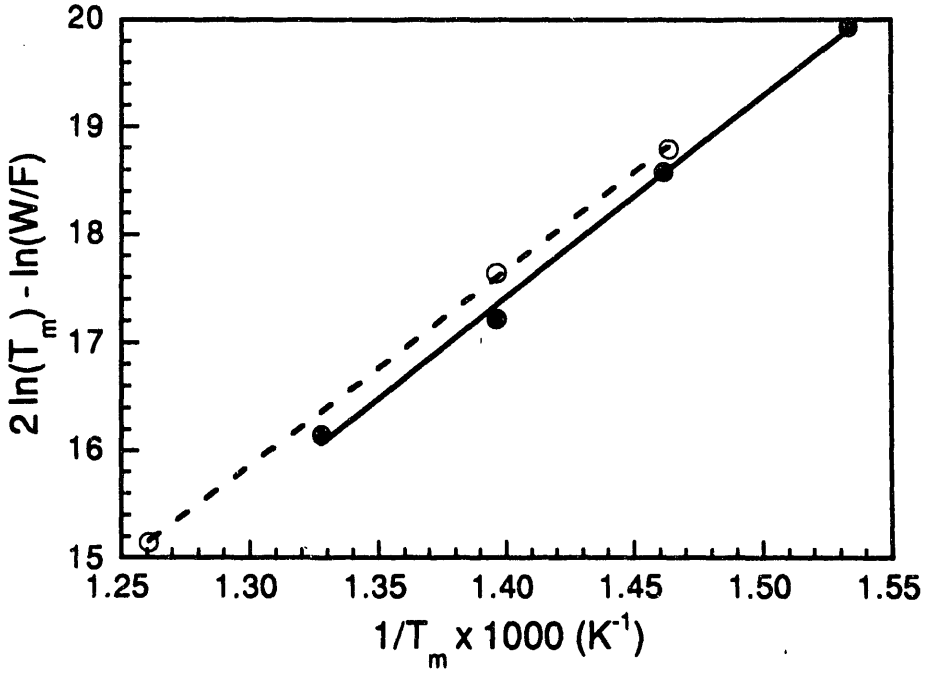

Figure 6. Temperature-programmed desorption results for ammonia from H-mordenite collected at different flow rates and sample weights. (o) 0.42 cm^3/sec (•) 1.25 cm^3/sec

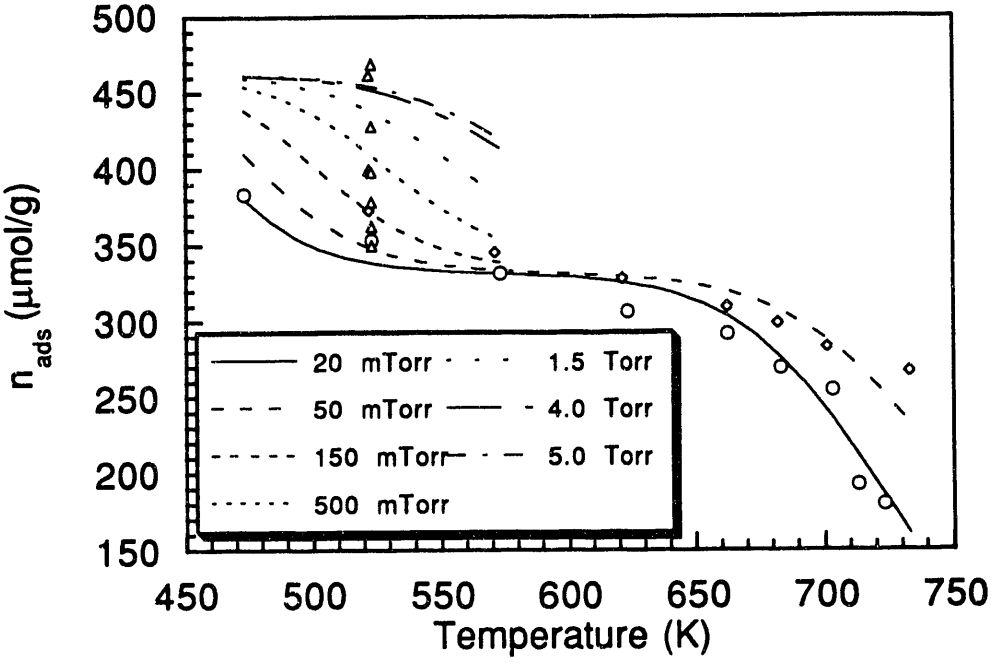

Figure 7. Pyridine uptakes on H-ZSM-5 measured by thermogravimetry as isobars at 20 mTorr (o) and 50 mTorr (◊), and an isotherm at 523 K (Δ). Fits of the data by combination of Langmuir isotherms appear as lines.

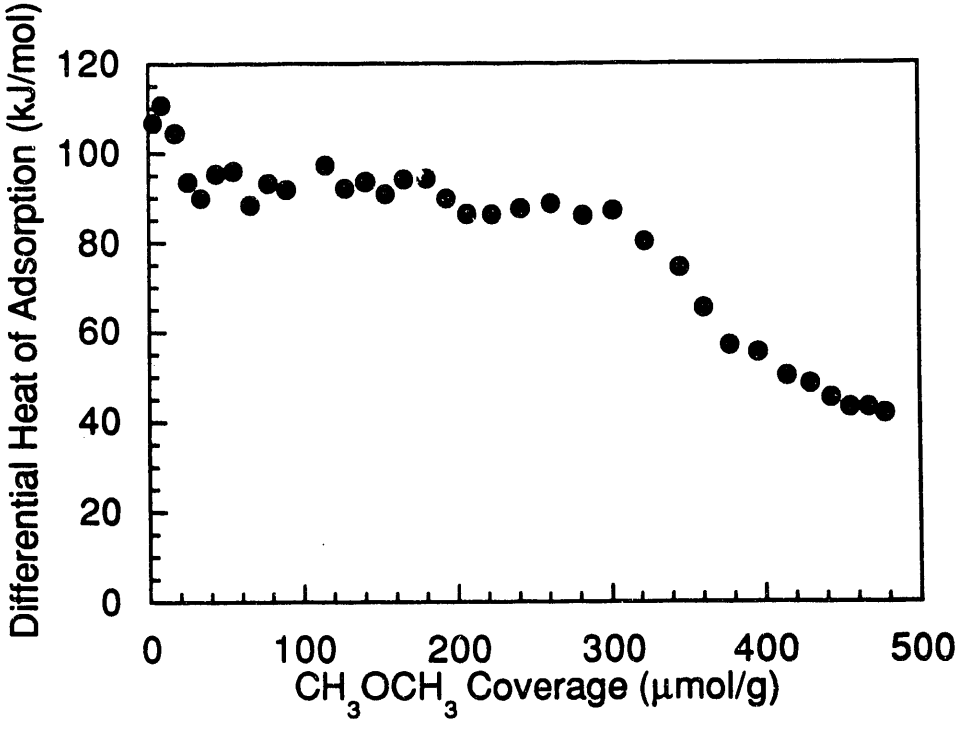

Figure 8. Differential heat of dimethyl ether adsorption versus dimethyl ether coverage on H-ZSM-5 at 473 K.

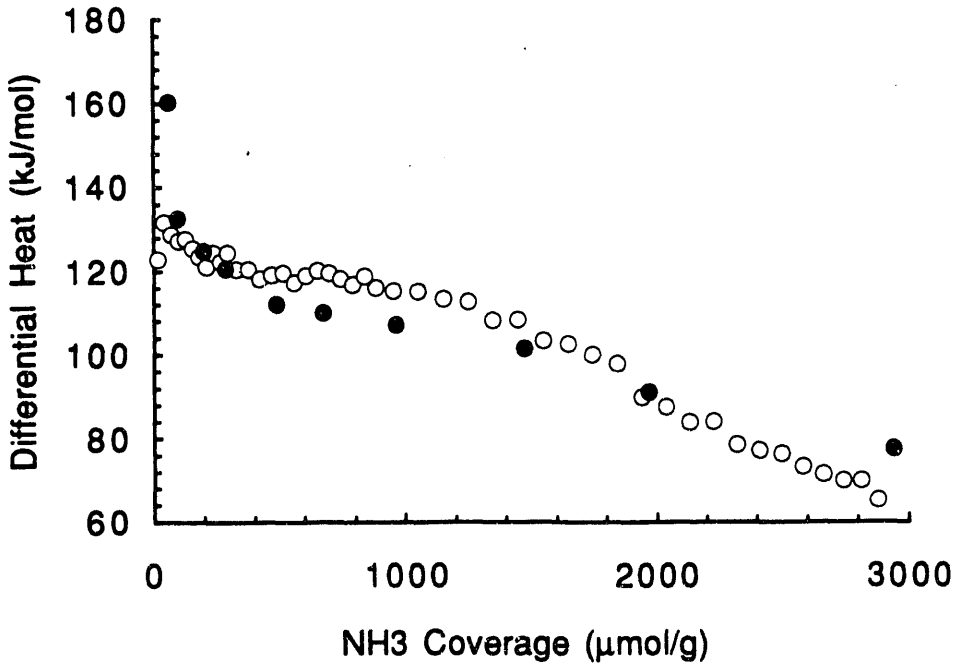

Figure 9. Differential heat of ammonia adsorption versus ammonia coverage on HNa-Y zeolite at 423 K with 82 % of the Na exchange cations replaced by protons (o). Results from thermogravimetric measurements by Boudart [3] and co-workers (•) are shown for comparison.

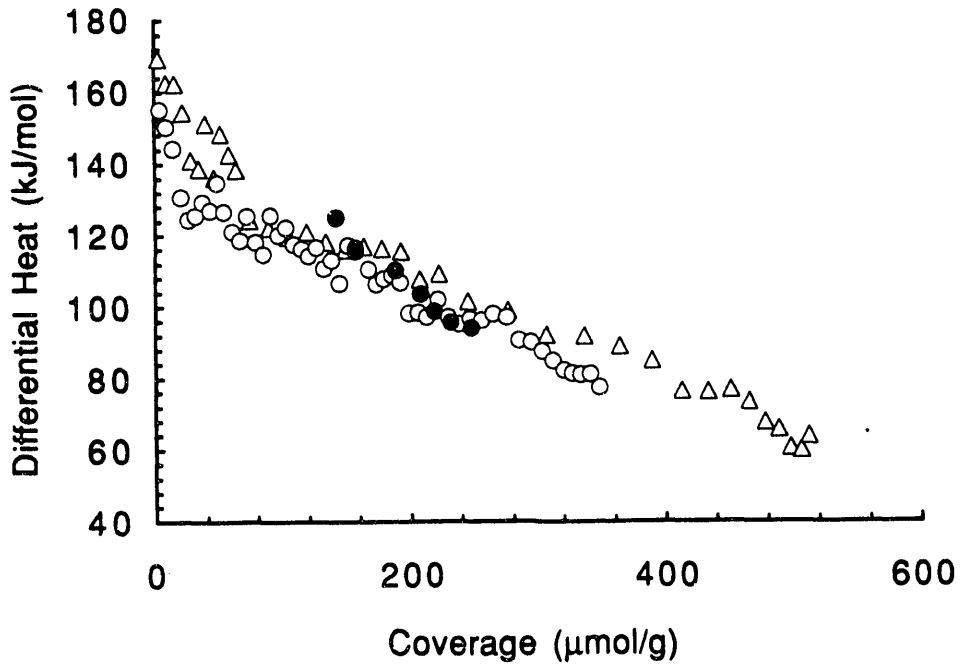

Figure 10. Differential heat of adsorption versus coverage for ammonia at 423 K (Δ), and pyridine at 473 K (o) on γ-alumina. Results from thermogravimetric measurements by Deeba and Hall [1] (•) are shown for comparison.

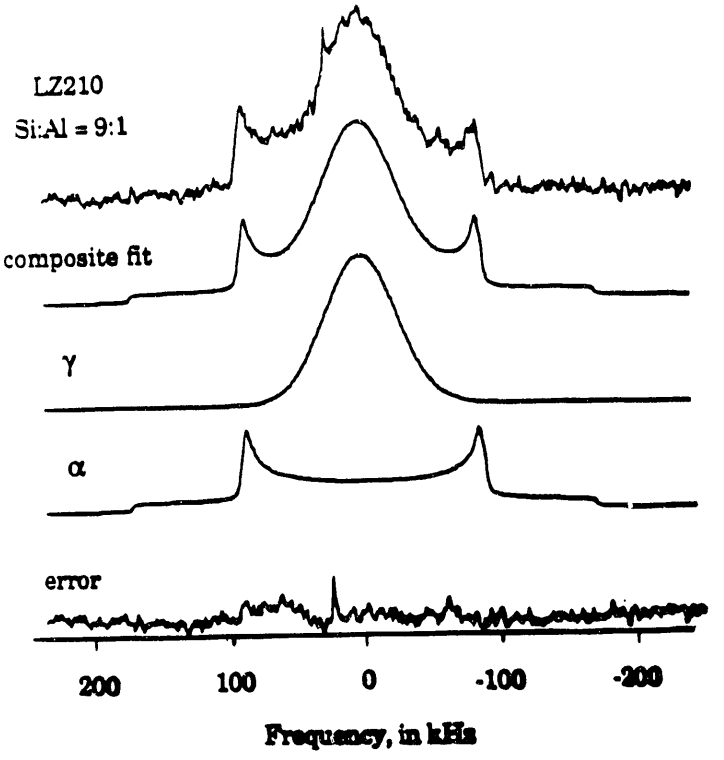

Figure 11. ^{2}D NMR spectra of (a) D-Y zeolite (1024 scans), (b) composite fit, sum of (c) and (d), (c) Gaussian peak: 63.1 kHz FWHH, 54% of area, (d) quadrupolar pattern: QCC=234 kHz, η=0.03, 46% of area, (e) difference between spectrum and fit.

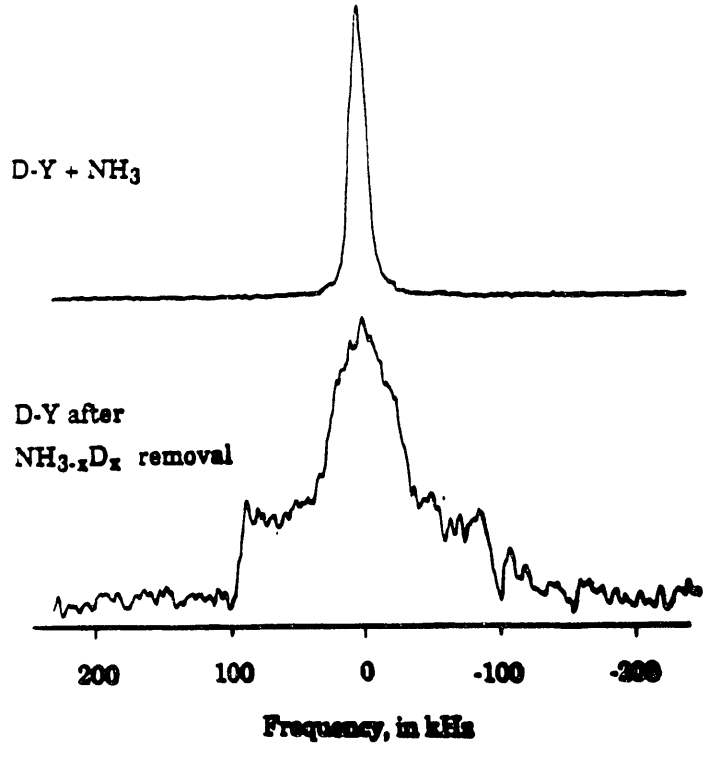

Figure 12. ^{2}D NMR spectra and fits of (i) D-Y zeolite after adsorption of NH_3 (624 scans: 76% Gaussian, 13.3 kHz FWHH; 24 % Gaussian, 48.1 kHz FWHH), and (ii) same sample after evacuation at 450°C to desorb ammonia (16587 scans: 53% Gaussian, 59.5 kHz FWHH; 47% quadrupolar pattern, QCC=234 kHz, η=0).

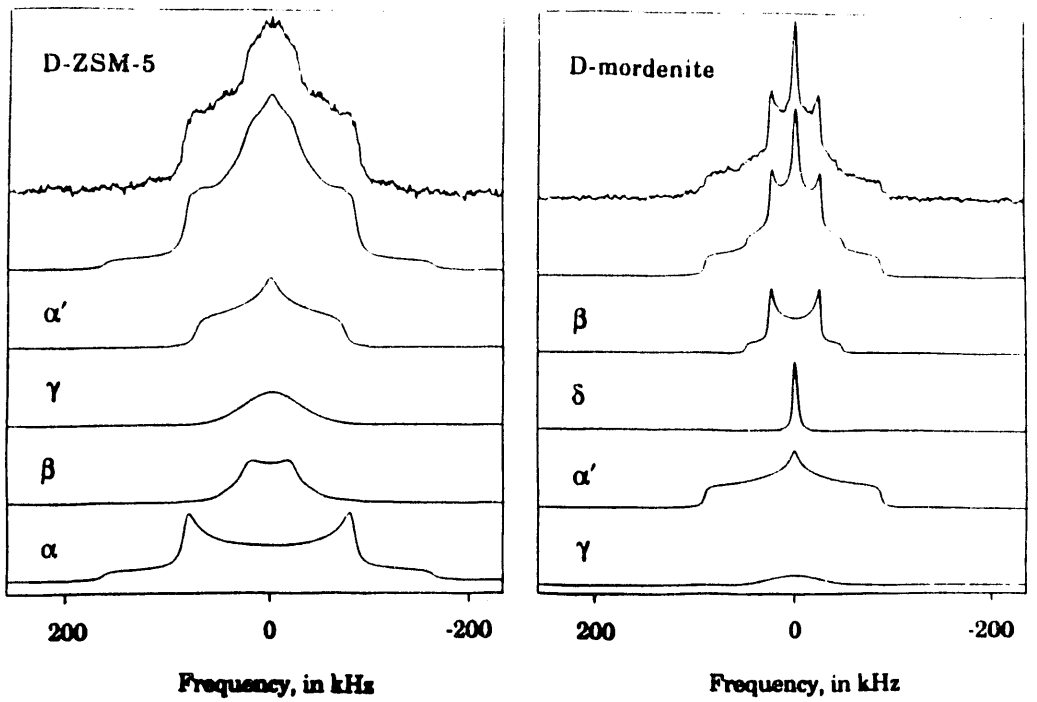

Figure 13. ^{2}D NMR spectra and fits for D-ZSM-5 and D-mordenite. D-ZSM-5 is fitted by (α') QCC=100 kHz, η=1, 31% of area, (γ) 65 kHz FWHH, 8% of area, (β) QCC=64 kHz, η=0, 15% of area, and (α) QCC=219 kHz, η=0, 46% of area. D-mordenite is fitted by (β) QCC=67 kHz, η=0, 30% of area, (δ) 6 kHz FWHH, 6% of area, (α') QCC=120 kHz, η=1, 55% of area, and (γ) 60 kHz FWHH, 9% of area.

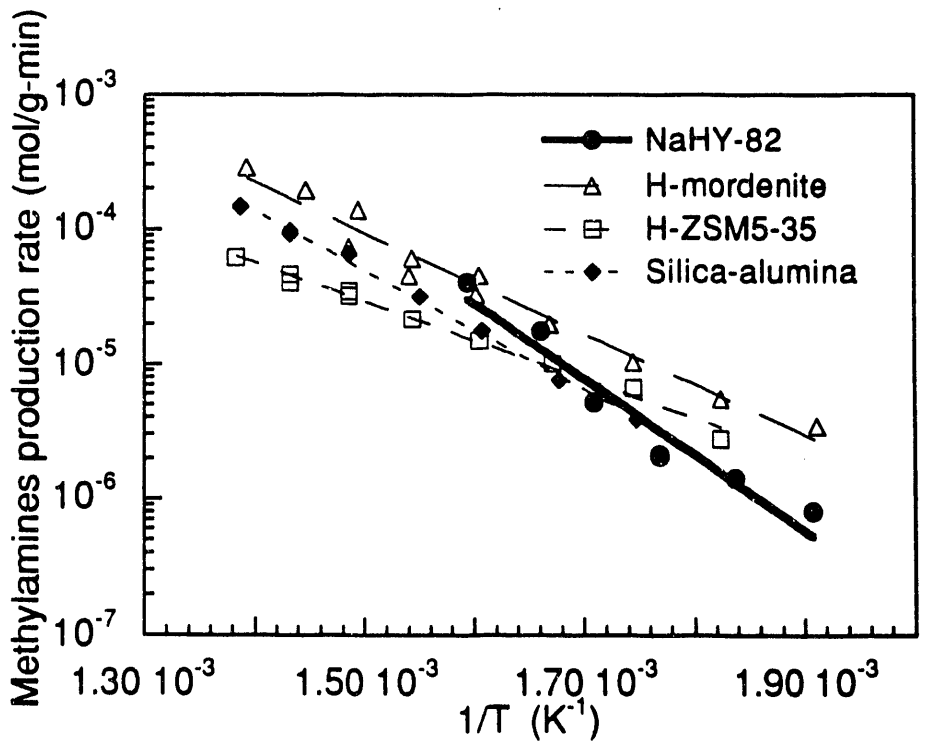

Figure 14. Arrhenius plots for total methylamine production on NaHY-82 (•), H-mordenite (Δ), SAC (♦), and H-ZSM-5-35.

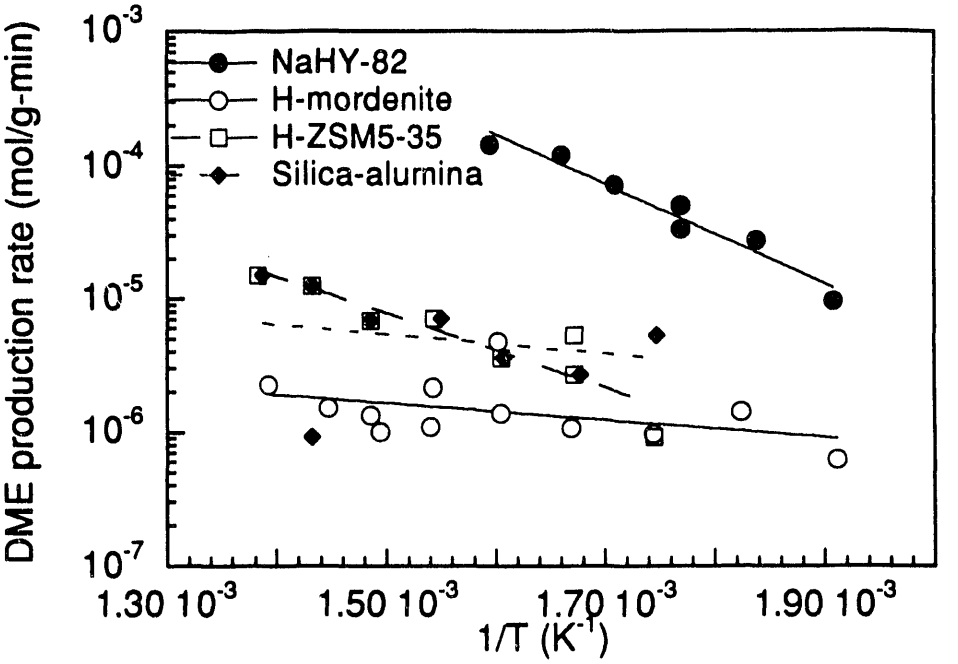

Figure 15. Arrhenius plots for DME production on NaHY-82 (•), H-mordenite (o), SAC (♦), and H-ZSM-5-35.

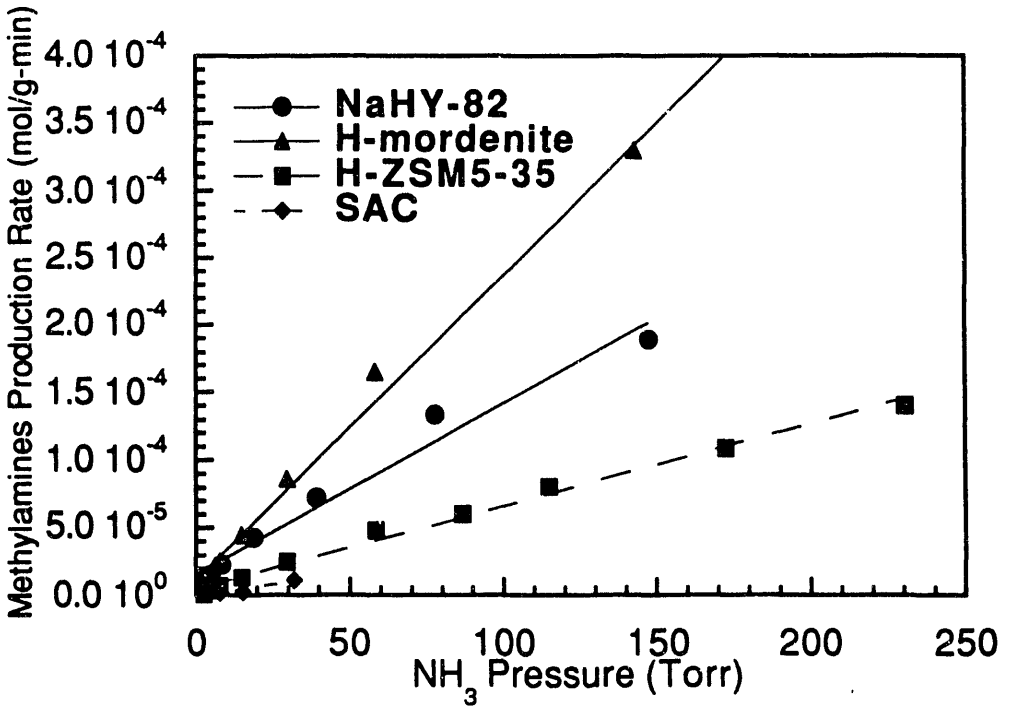

Figure 16. Dependence of methylamine production rate on ammonia partial pressure.

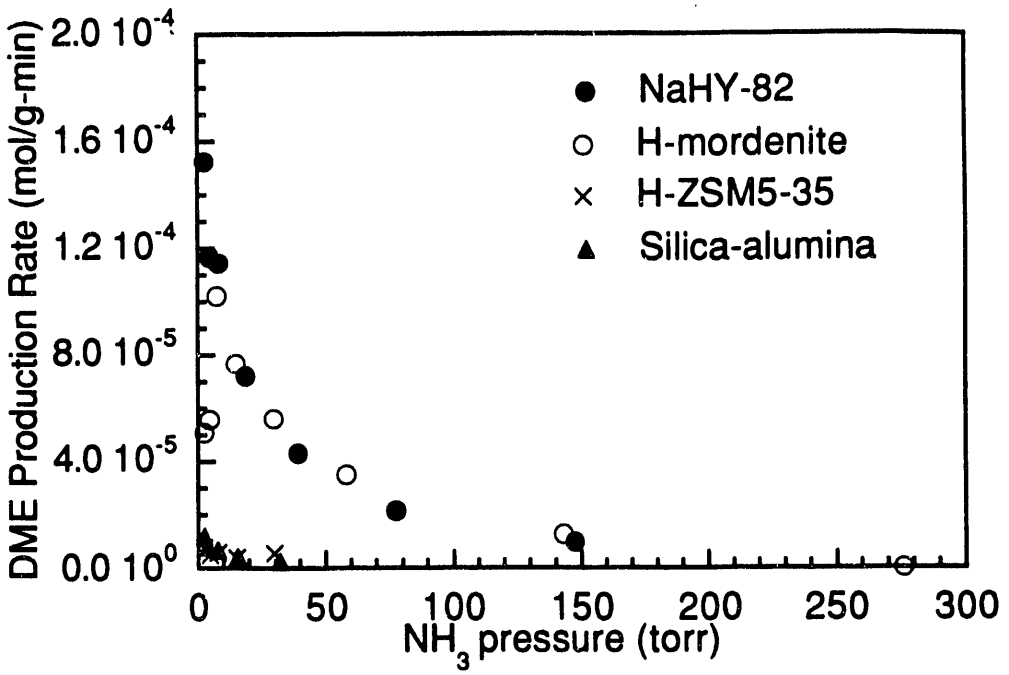

Figure 17. Dependence of DME production rate on ammonia partial pressure.

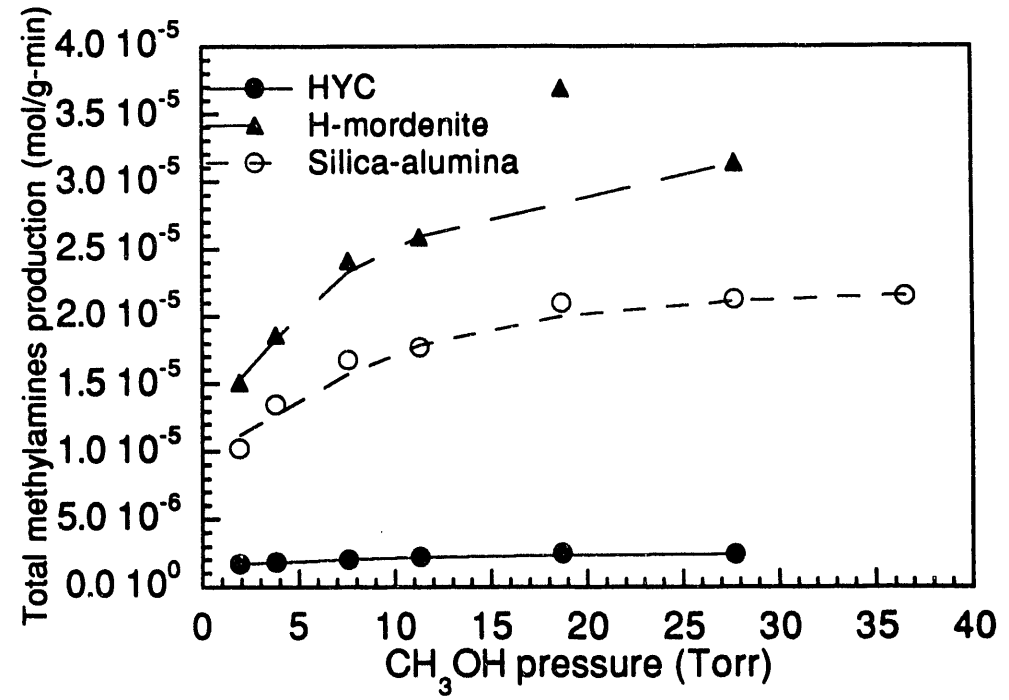

Figure 18. Dependence of methylamine production rate on methanol partial pressure for HYC (•), H-mordenite (Δ), and SAC (o).

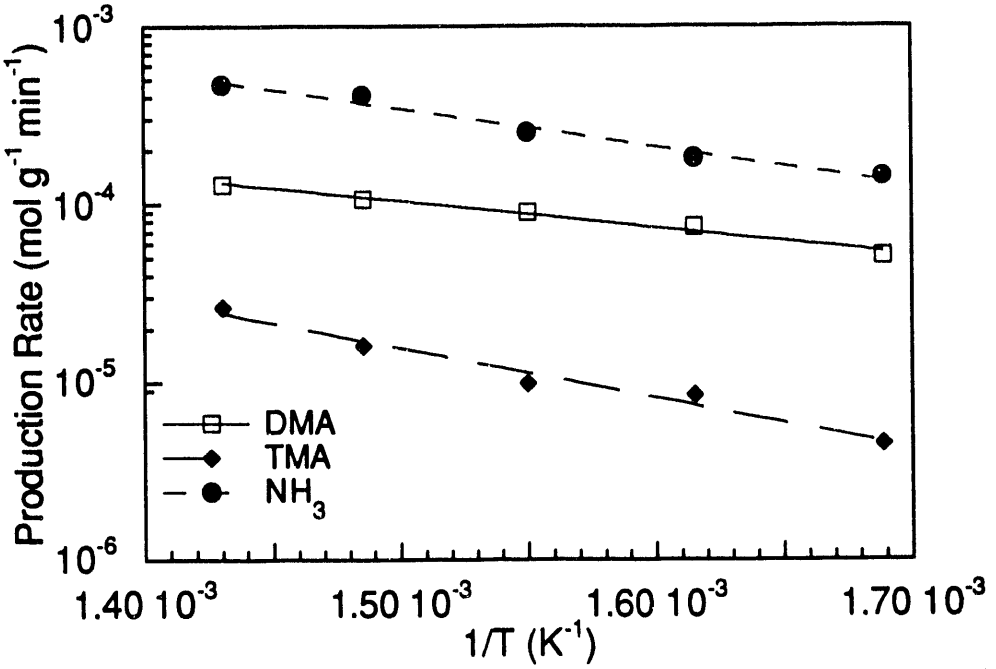

Figure 19. Arrhenius plot for MMA disproportionation on H-ZSM-5.

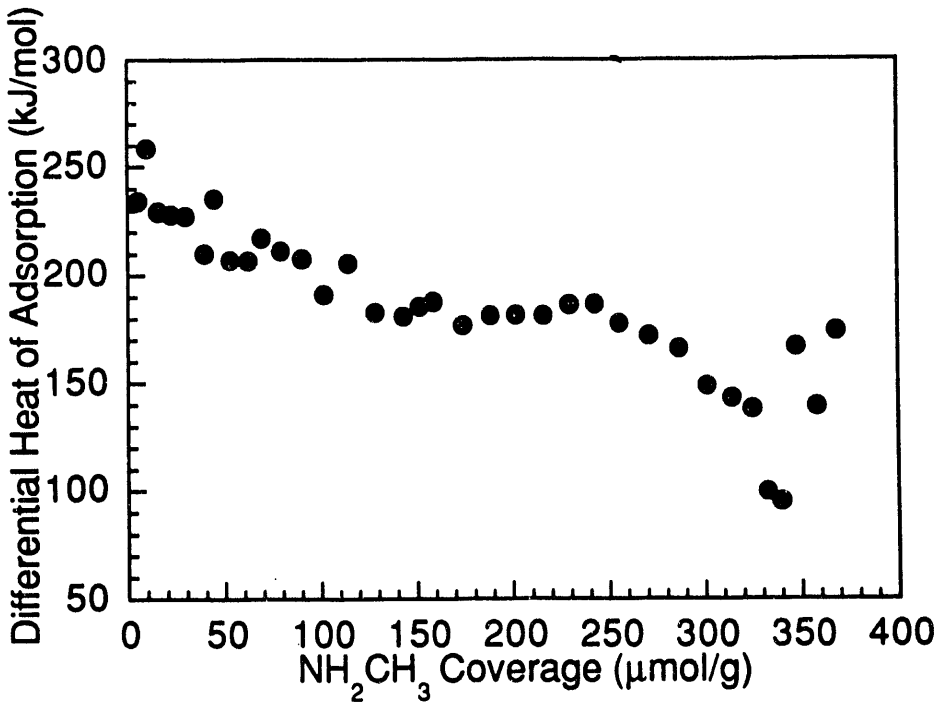

Figure 20. Differential heat of monomethylamine adsorption versus monomethylamine coverage on H-ZSM-5 at 473 K.

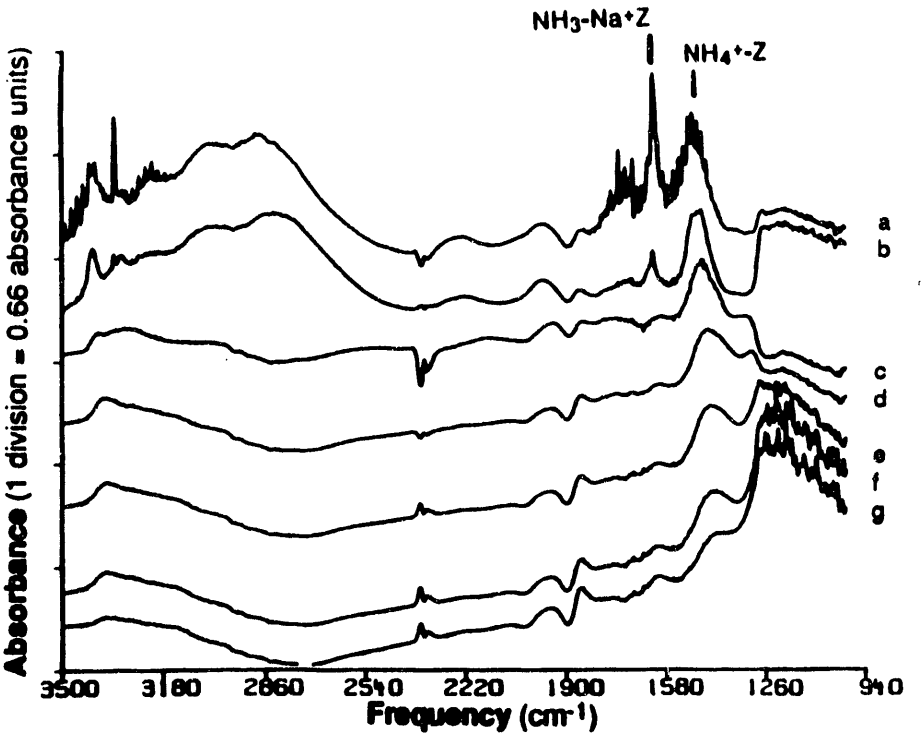

Figure 21. Infrared spectra for NH_3 region for (a) NH_3 at 7 Torr and room temperature, (b) after purging with He at room temperature, and (c) 373 K, (d) 473 K, (e) 523 K, (f) 573 K, and (g) 623 K.

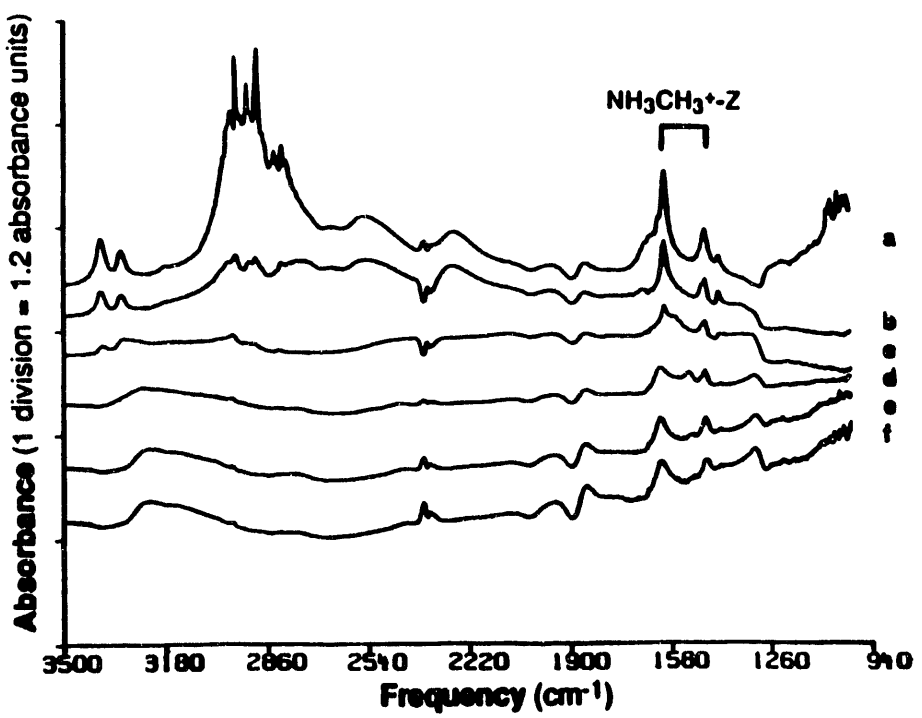

Figure 22. Infrared spectra for MMA region for (a) MMA at 7 Torr and room temperature, (b) after purging with He at room temperature, and (c) 373 K, (d) 473 K, (e) 573 K, and (f) 673 K.

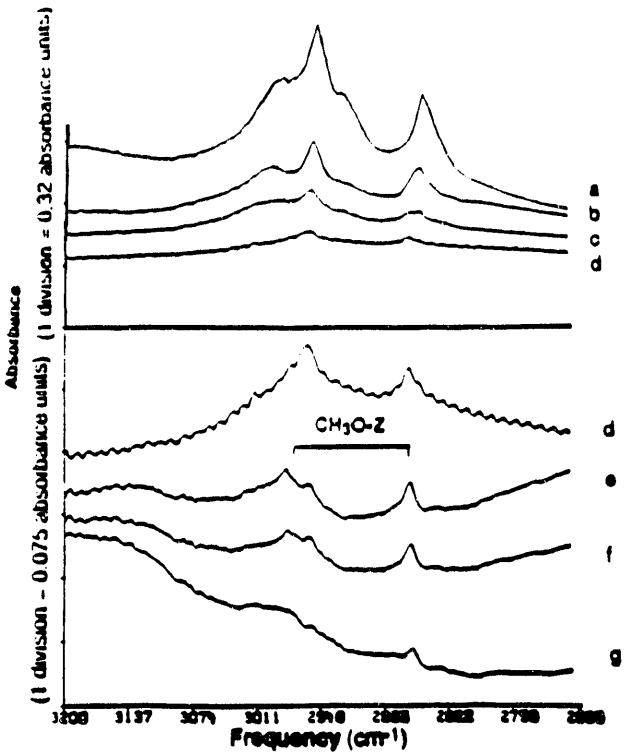

Figure 23. Infrared spectra for methanol region for (a) CH_3OH at 7 Torr and room temperature, (b) after purging with He at room temperature, and (c) 373 K, (d) 473 K, (e) 523 K, (f) 573 K, and (g) 623 K.

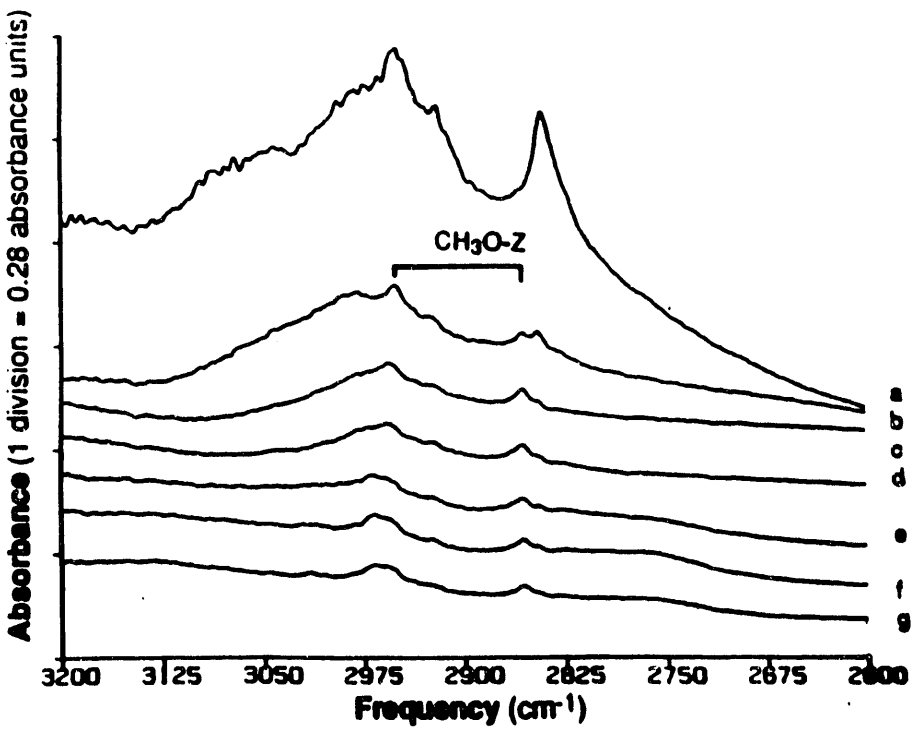

Figure 24. Infrared spectra for methanol region for (a) CH_3OH at 10 Torr and NH_3 at 7 Torr and room temperature and at (b) 373 K, (c) 473 K, (d) 523 K, (e) 573 K, (f) 623 K, and (g) 673 K.

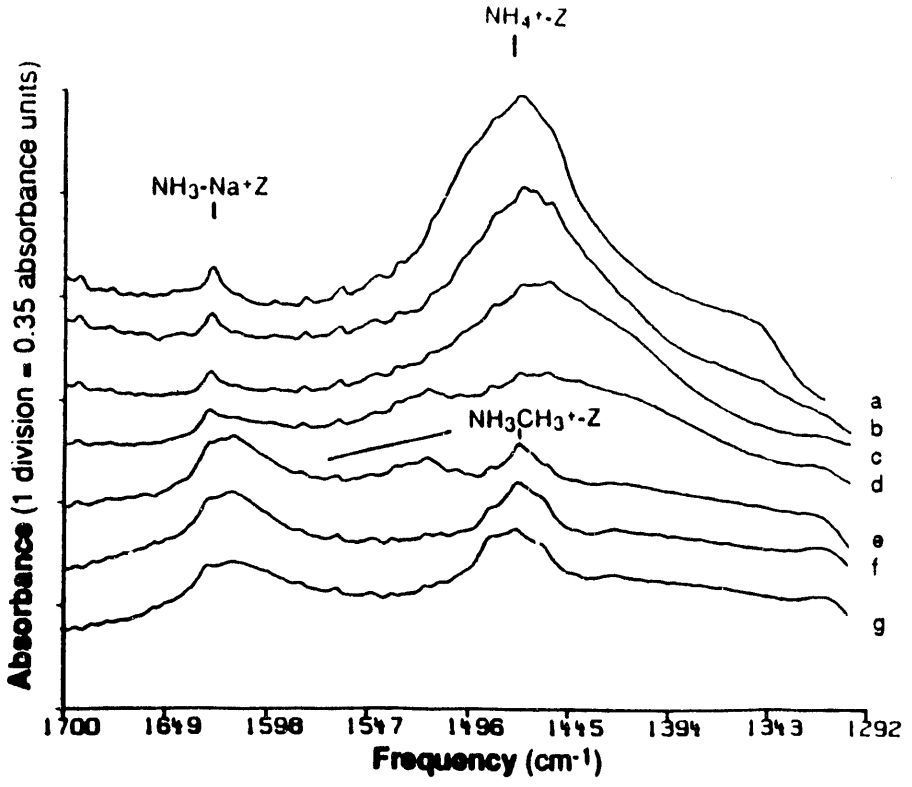

Figure 25. Infrared spectra for NH_3 and MMA region for (a) CH_3OH at 10 Torr and NH_3 at 7 Torr and room temperature and at (b) 373 K, (c) 473 K, (d) 523 K, (e) 573 K, (f) 623 K, and (g) 673 K.

DATE
FILMED
7/22/93
END